POLITECNICO DI TORINO

Master's Degree in Civil Engineering

Master's Degree Thesis

Flexural behaviour of GFRP reinforced concrete beams

Supervisor

Prof. Alessandro Pasquale Fantilli

Candidate

Khizer Hayat

Abstract

Reinforced concrete has been used for structures for a long time, mainly steel reinforced concrete. An alternative is required since steel has some flaws. One of the most significant defect of the steel is corrosion, which shortens the life of steel reinforced structures, it results in repairing costs etc. Furthermore, steel is not eco-friendly at all, a ton of steel production produces 1.89 tons of CO2 as byproduct. Alternatives, including as GFRP, BFRP, AFRP, and CFRP bars, are available and being produced for use as internal reinforcement, although they are not widely used. The reason for this is the cost of some of these materials, such as CFRP, which is almost 30 times more expensive than steel. For others very little research has been done on concrete reinforced with these materials, with respect to steel reinforced beams, for which there is not any doubts on how to design. In this study, empirical formulas for flexure design of GFRP reinforced beams is derived. For this purpose publications from literature were analyzed, and data on GFRP-reinforced beams tested in bending with 3 or 4 point bending tests were gathered. The formula is derived by numerical simulations, using moment-curvature relationship. This formula is then validated by comparing it to the experimental results from these tests.

Dedicated to my father and mother, who overcame adversity
to shape me into the person I am.
Dedicated to my son, who showed me a new dimension of love
and dedication to me that I had not known existed
before his birth.

Acknowledgements

First of all, **alhamoLillah**, I would like to praise Allah the Almighty, the Most Gracious, and the Most Merciful for all His blessing on me.

I'd like to express my gratitude to my family:

My parents deserve special thanks for their love, emotional and financial support. I always knew that you believed in me and wanted the best for me. You have helped me through difficult times.

Special thanks to my siblings and my wife, for being by my side during these years.

A special thanks to my many friends for their support.

My sincerest thanks are extended to my supervisor and mentor, Professor Alessandro Pasquale Fantilli, for his guidance. I would also like to thank all of my teachers for all of their academic and life's lessons.

Table of Contents

List of Tables vii

List of Figures viii

Acronyms & Notations xi

1 Introduction 1

1.1 General aspects . . . 1
1.2 Steel corrosion in R.C. . . . 2
1.3 Increasingly expensive and inaccessible steel . . . 3
1.4 GFRP bars properties . . . 8
1.5 Sustainability . . . 14
1.6 Research significance and limitations . . . 17
1.7 Method . . . 18

2 Flexural behaviour of GFRP reinforced beams 20

2.1 Tests on GFRP beams . . . 21
2.1.1 El-Nemr et. al. . . . 21
2.1.2 M. Pecce et. al. . . . 28
2.1.3 A. Ramachandra Murthy et. al. . . . 29
2.1.4 Sehab Mehany et. al. . . . 32
2.1.5 H. Falah Hassan et. al. . . . 37
2.1.6 Mohamed S. Moawad & Ahmad Fawzi . . . 39
2.1.7 Sungwoo Shin et. al. . . . 43
2.2 Summary and conclusions . . . 46

3 Parallel between GFRP reinforced concrete and steel reinforced concrete 49
3.1 Calculation models for GFRP reinforced concrete beams 53
3.1.1 Relationship between ω and ξ for GFRP reinforced beams 58
3.1.2 Relationship between μ_{Rd} and ξ for GFRP reinforced beams 59
3.1.3 Resisting moment formulation for GFRP reinforced beams 60
3.1.4 Relationship between μ_{Rd} and ω 62

4 The comparison between the computation model and the experimental results 64

5 Conclusions 69

Bibliography 71

List of Tables

2.1 GFRP properties, El-Nemr [17] 22
2.2 Test specimens details 1, El-Nemr et. al. [17] 23
2.3 Test specimens details El-Nemr et. al. [17] 24
2.4 Cracking and Ultimate Moments, El-Nemr et. al, [17] . 25
2.5 Test specimens details, A. Ramachandra M. et. al. [19] 30
2.6 Test specimens details, average values A. Ramachandra M. et. al. [19] 31
2.7 GFRP properties 1, Shehab Mehany et. al. [20] 33
2.8 GFRP properties 2, Shehab Mehany et. al. [20] 33
2.9 Specimens details , Sehab Mehany et. al. [20] 34
2.10 Test results, Sehab Mehany et. al. [20] 34
2.11 GFRP bars specifications 37
2.12 Specimens details, H. Falah Hassan et. al.[21] 38
2.13 Specimens details, M. S. Moawad, A. Fawzi [22] 40
2.14 Tests results, M. S. Moawad, A. Fawzi [22] 41
2.15 Load deflection, M. S. Moawad, A. Fawzi [22] 41
2.16 Reinforcement characteristics, Sungwoo Shin et.al. [23] 43
2.17 Specimens details, Sungwoo shin et. al. [23] 44
2.18 Load and deflection,Sungwoo shin et. al. [23] 44
2.19 Collected data summarized 48

3.1 Data collected from articles 56
3.2 Calculated variables for numerical simulation 57

List of Figures

1.1 Europe Hot Rolled Coil Price [1] 4
1.2 China Iron Ore Import Price [1] 6
1.3 China Hot Rolled Coil Export Price [1] 7
1.4 Composition of FRP[6] 9
1.5 FRP types [6] 10
1.6 Pultrusion process [7] 10
1.7 Comparison between GFRP and steel [9] 13

2.1 Types of reinforcing bars [17] 22
2.2 Beams geometry, El-Nemr et. al. [17] 24
2.3 Deflection vs. applied moment plot 1, El-Nemr et. al. [17] 26
2.4 Deflection vs. applied moment plot 2, El-Nemr et. al. [17] 27
2.5 Beams geometry, M. Pecce et. al. [18] 28
2.6 Test results, M. Pecce et. al. [18] 29
2.7 Beams geometry, Ramachandra et. al. [19] 30
2.8 Load deflection curves GFRP 13 mm reinforced beams, Ramachandra et. al. [19] 31
2.9 Average load deflection curves, Ramachandra et. al. [19] 32
2.10 Types of reinforcing bars, Sehab Mehany et. al. [20] . . 33
2.11 Specimens Geometry , Sehab Mehany et. al. [20] . . . 35
2.12 Moment deflection curves, Sehab Mehany et. al. [20] . 36
2.13 Beams geometry, H. Falah H. et. al. [21] 38
2.14 Load deflection curve, H. Falah H. et. al. [21] 39
2.15 Beams geometry, M. S. Moawad, A. Fawzi [22] 40
2.16 Load-deflection curves, M. S. Moawad, A. Fawzi [22] . 42
2.17 Beams Geometry, Sungwoo shin et. al. [23] 43

2.18 Loaad-deflection curves, Sungwoo shin et. al. [23] . . . 45

3.1 Load deflection of beam with different reinforcements . 50
3.2 Neutral axis position coefficient 51
3.3 Field 3 configuration 52
3.4 Reinforcement percentage - Neutral axis coefficient plot 58
3.5 Curvature (μ) - Neutral axis coefficient (ξ) plot 59
3.6 Simplified configuration 61
3.7 $\mu - \omega$ relationship for GFRP 63

4.1 $\mu - \omega$ comparison with experimental data 65
4.2 $\mu_{Rd} - \omega$ comparison with experimental data 66
4.3 $M_{R,th} - M_{exp.}$ plot 67
4.4 $M_{R,moment-curvature} - M_{exp.}$ plot 68

Acronyms & Notations

FRP Fiber Reinforced Polymers

CFRP Carborn Fiber Reinforced Polymers

AFRP Aramid Fiber Reinforced Polymers

GFRP Glass Fiber Reinforced Polymers

C.C. Concrete Compression Failure

f_{fu} Ultimate tensile strength of GFRP bars
Ef Elastic Modulus of GFRP bars
Af GFRP Bars Area
ρ_f Reinforcement Ratio
$\rho_f b$ Balanced Reinforcement Ratio
M_{cr} Cracking Moment
$f'c$ Concrete Compressive strength
σ_c Concrete Compressive strength
A_S Steel Reinforcement Area
ξ Neutral Axis Position Coefficient
y_0 Neutral Axis Position
d Distance To The Reinforcement
ω Percentage Of The Reinforcement
μ_{Rd} Design Resisting Curvature

Chapter 1

Introduction

1.1 General aspects

Concrete has been used for construction for thousands of years, and its properties have evolved over time, with one of the most significant changes being the discovery of tensile reinforcement. For decades, rebar, also known as reinforcing steel or reinforcement bars, has been used in construction. Steel rebar is the champion of reinforcements in reinforced concrete due to its variety of sizes and applications, tensile strength, and unrivaled ductility. However, steel has some flaws, such as corrosion, therefor, an alternative reinforcement is needed.

1.2 Steel corrosion in R.C.

One of the common defects associated with the use of conventional steel bar reinforcement is corrosion, which shortens the lifetime serviceability of the concrete structure.

The alkaline environment in the concrete protects the steel rebar from corrosion. When a structure is not exposed to an aggressive environment, has sufficient concrete cover, a low number of cracks, and good concrete quality, this protection is usually sufficient. For instance, the reinforcement can corrodes over time due to a decrease in alkalinity in the concrete, caused by carbonation, which usually occurs in severe conditions.

Corrosion of steel rebar results in a loss in cross-sectional area, concrete spalling due to the expansion that follow rust formation. Furthermore the possibility of losing adhesion of the reinforcement to the surrounding damaged concrete, which can affect the functionality of reinforced concrete structures or even their structural stability.

1.3 Increasingly expensive and inaccessible steel

Another reason why an alternative reinforcement is needed, and it is needed as soon as possible, is the continuously increasing price of steel. The steel price is currently standing at all time high record and is still increasing.

The increased price of the steel, due to pandemic, is now increasing due to the recent war between Russia and Ukraine. To gain a better understanding, the price of hot-rolled coil is currently around 1150 $EUR/tonne$ which means it has climbed by more than 250 % since 2020, when it was nearly the average cost of the preceding decade, which was also higher than the previous decade. It is also significantly higher than the price reached during the 2008 financial crisis as well (almost 1.5 times) see figure 1.1.

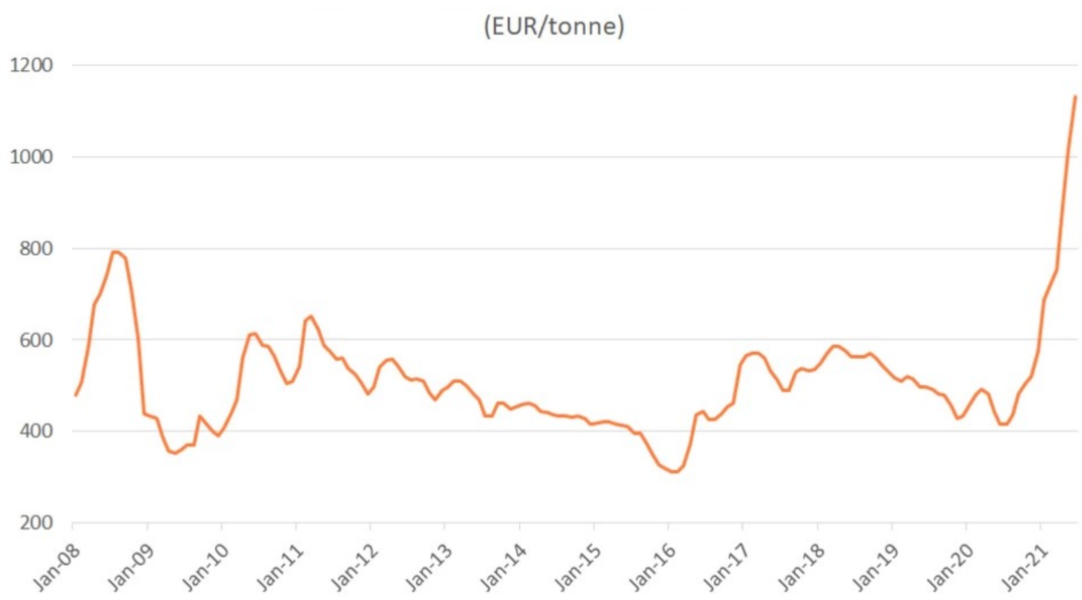

Figure 1.1: Europe Hot Rolled Coil Price [1]

The figure 1.1 highlight the different "events" and their effects. Other steel products price trend is similar to this. In chronological order we have around 2008 the financial crisis effects, the increase in price and the "fast" control over it thanks to the European policies. Steel overproduction issue of China and their attempt to overtake the European steel market with their cheap prices. European attempt to stop this with restrictions which effects can be seen starting from 2016, indeed we have the European steel price recovery.

Deterioration of the of the steel price due to weakening of the steel consumption, specially in the automotive sector, and the oversupply pressure, after reaching a high point in early 2018. [1]

Finally, an unusual slope can be seen starting from mid 2020, which is obviously due to the Covid pandemic. Some more words should be spent here to have a better understanding of what really happened. Because of the uncertainty in demand and the need for companies to generate cash, destocking was done throughout the supply chain. Steel mills were compelled to decrease output due to lower orders. Low stockpiles and earlier steel production cuts pushed European prices higher at the start of 2020, creating a fragile sense of optimism.

Suddenly Covid 19 pandemic hit, which fueled unfavorable attitude. As governments attempted to contain the spread of the virus, lock-downs were implemented, and economic activity fell. Despite growing Covid cases in Europe, the steel market began to recover. Following lock-downs, steel-intensive end-user industries were able to continue operating, and sentiment improved.

Steel demand began to recover, but supply was drastically cut. European mills have made significant output cuts by the middle of 2020. The ensuing delayed ramp up of manufacturing was due to a number of issues. Steelmakers faced a variety of technical challenges in resuming production, while social distance created limits for plant workers. Mills failed to access required raw materials due to supply chain interruptions, including container shortages, rising transport costs, and port delays.

The strong overproduction of China pushed up the price of iron ore, see figure 1.2 [1].

Figure 1.2: China Iron Ore Import Price [1]

Furthermore, the non-normal uptrend of the steel price, (Hot rolled coil which reflects the steel products price) can be seen by the figure 1.3, which somehow represent the Chinese aggressive government fiscal and monetary policies [1]

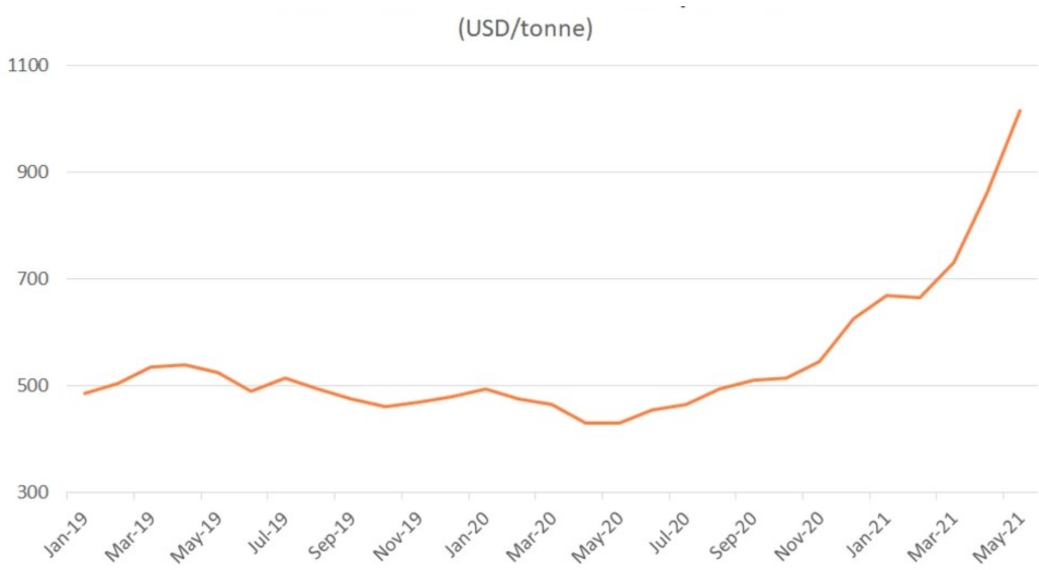

Figure 1.3: China Hot Rolled Coil Export Price [1]

Mills in Europe were hesitant to restore production quickly for fear of jeopardizing the steel price rebound and possibly being left with excess supply if demand went off again. Steelmakers' fear were unfounded, since demand from end-users grew steadily. Here we witnessed **steel shortage**. [1].

The most recent addition to the list of events is the conflict in Ukraine, which will have a direct impact on steel pricing in Europe, as Russia and Ukraine were two of the main suppliers of steel raw materials and semi-finished steel products. And there will be an indirect influence because energy prices are projected to rise, which are already at record highs. To give some numbers, Italy imported 5.18 tons of steel from

Ukraine. [2]. Furthermore, 41.1% of gas and 36.5% of the fuel in Europe is imported from the Russia [3], we have already seen a 106 % increase in gas prices and a 22 % increase in petrol prices [4].According to the United Nations Comtrade, the European Union imported $8.77 billion worth of iron and steel from Russia in 2021[5]. The prices will undoubtedly rise, as the consequences, particularly the indirect ones, take time to manifest. **Therefore, an alternative reinforcement is needed.**

1.4 GFRP bars properties

Glass Fiber-Reinforced Polymer (GFRP) bars are one of the alternative reinforcements used to overcome the defects in the conventionally reinforced concrete structural members.

Fiber Reinforced Polymers (FRPs) are a type of composite material that is made up of a polymer matrix reinforced with fibers. Where usually the fibers are almost the 65% of it and the rest is the polymer matrix. An epoxy resin is commonly used as the polymer matrix, which enables bonding to the fibers, the figure 1.4 depicts an illustration. Furthermore, it transfers stresses to the fibers, prevents fiber damage while the bars are stored, transported, and even during service life.

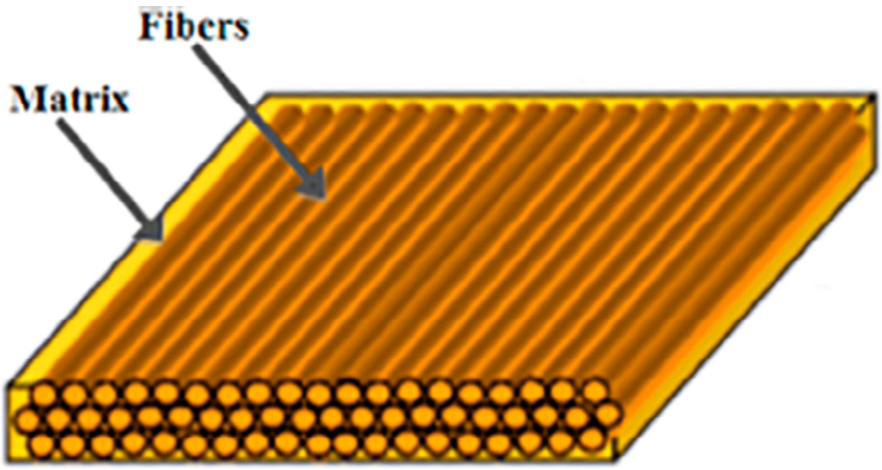

Figure 1.4: Composition of FRP[6]

FRP reinforced with Glass, Aramid or Carbon fibers, referred to GFRP, AFRP and CFRP respectively, are the most extensively used alternative reinforcing elements in the construction sector, shown in the figure 1.5.

Because of their abundance and low cost, GFRP bars are the most popular of these FRP reinforcement bar types.
FRP are usually produced by pultrusion, which consist of roving, resin bath, resin control, preforming, heated die to give the desired surface shape, pulling and cutting, a scheme is shown in the figure 1.6:

Figure 1.5: FRP types [6]

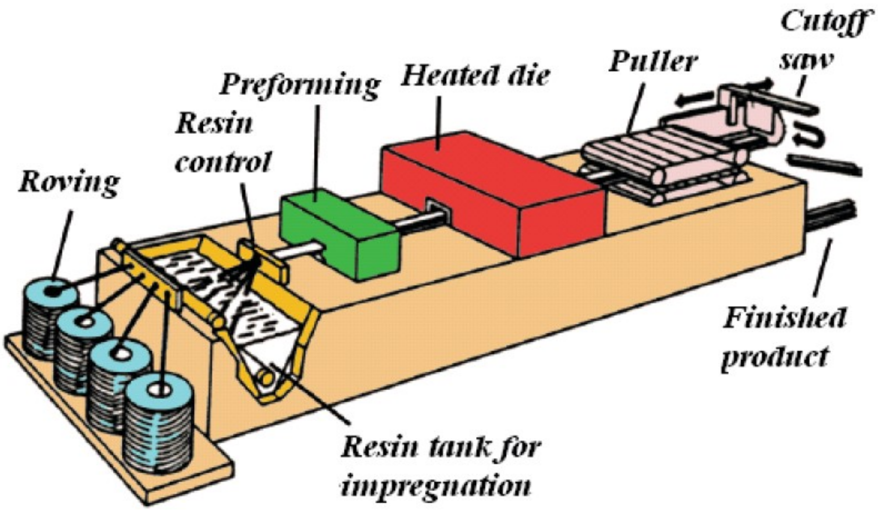

Figure 1.6: Pultrusion process [7]

FRP bars are potentially useful for constructions exposed to very aggressive environments, such as marine environments or situations where de-icing salts are used extensively, such as infrastructure in cold areas or high mountains, as they are not susceptible to corrosion.
FRPs were at first developed and used in the aerospace, aeronautics, naval and automotive sectors, are known specially for their strength and durability.

Lower weight to strength ratio, high longitudinal tensile strength, non-magnetic properties and specially corrosion and chemical resistance are some of the benefits of FRP reinforcement bars over steel reinforcement. Being the stiffness almost the half of the steel, the crack in the reinforced beam will be almost the double.

One of the disadvantages, regarding the durability, of the GFRP bars is the reactivity of GFRP composites in an alkaline environment, such as concrete, which can be prevented by using GFRP made of specific polymer matrix:

A concrete environment is typically alkaline, with a pH ranging from 12 to 13 depending on the concrete design mixture and the type of cement employed. Glass fibers suffer from loss of toughness and strength, as well as embrittlement, in this alkaline environment. Glass fibers are harmed by a combination of two processes chemical attack by the alkaline cement environment on the glass fibers and the concentration and proliferation of hydration products between filaments. In the presence of moisture, hydroxylation, which is an oxidation of carbon-hydrogen bonds into carbon-hydroxyl, can create fiber surface pitting and roughness, which act as faults that severely decrease fiber characteristics. Furthermore, the ions calcium, sodium, and potassium in the concrete pore solution are extremely aggressive towards glass fibers. As a result, glass fiber deterioration is caused by a mix of alkali salts, pH, and moisture, rather than only a high pH level [8].

To prevent these issues the FRP having certain resin matrixes shell be used, i.e. vinyl-ester, epoxy. which are reported to be more suitable for this purpose. These resins provides enough toughness to prevent the development of micro-cracks. Furthermore, vinyl-ester resins are resistant to a wide range of acids [8].
Other disadvantages are lower elasticity module compared to steel, and linear elastic behaviour till failure, they do not exhibit plastic behaviour, as it is shown in the figure 1.7.

GFRP weight way less than steel, for example, one meter of 8mm steel rebar weighs 0.4 kilos, while the same size GFRP bar is 0.08 kilos, making it five times lighter.

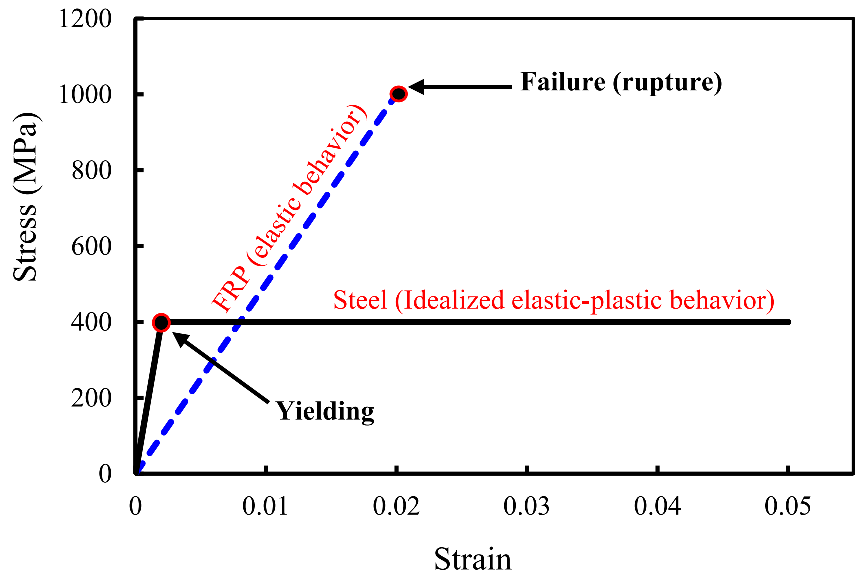

Figure 1.7: Comparison between GFRP and steel [9]

By comparing prices of 2021, which are the most recent accessible prices, steel and GFRP bars, for example, of the same sizes stated above (8mm), cost 0.12 Euros and 0.30 Euros per meter, respectively.

Despite the fact that FRP reinforcement bars are more expensive than steel reinforcement at first, their usage in structural components will greatly cut maintenance costs in aggressive environments, as well as overall damage repair costs. Steel reinforced concrete structures require some form of rehabilitation in as little as 5 to 10 years, and major rehabilitation in as little as 20 years. In USA, for example, the annual cost to owners of existing concrete structures for repair, protection, and strengthening is estimated to be between 18 and 21 billion dollars. Another cost to consider is the labor time cost, as GFRP is 5 times lighter in weight than steel, making laying and installation more efficient. GFRP reinforced structures can last way more longer than 100 years. For instance GFRP reinforced concrete slabs exposed to significant fatigue loads (such as driveways and bridge decks) are expected to crack less and last up to 20 times longer than comparable structures reinforced with conventional steel [10].

1.5 Sustainability

Steel is undoubtedly the most useful and widely used material in the world. It is used in practically every industry, from construction to mechanical, from motor cars to aerospace, and so on. Steel is the substance that has contributed the most to the technological and economic development that we know today. However, it is also one of the materials with the biggest impact on pollution emissions into the atmosphere throughout the production process.
Steel production contributes for 30% of annual pollution in terms of CO2, the principal polluting gas in the atmosphere, caused by global industrial activity [11].

According to World Steel Association calculations, an average of 1.89 tonnes of CO2 was emitted per tonne of steel produced in 2020, which means it is equal 190 percent of the production [12]. Looking back at prior years' publications, we can see that this value is almost the same

since a long time.
It is estimated that on average the steel industry generates between 7% and 9% of direct emissions from the global use of fossil fuel, this is because steel production requires large amounts of energy [13].

The steel sector utilizes around 20 GJ (5.6 MWh) per year on average, **with coal accounting for 75% of this consumption**. Steel production also results in enormous amounts of pollution being emitted. Steel production necessitates vast amounts of coke (a type of coal), which is tremendously harmful to the environment. Coke ovens create air pollution, including naphthalene, which is highly toxic and can cause cancer. Wastewater from the coking process is also highly toxic, containing cyanide, sulphides, ammonium, and ammonia, as well as various carcinogenic organic chemicals. Each year, approximately 67 billion tons of polluted water are released from raw material extraction and steel production[14].

GFRP is undeniably less harmful to the environment, when compared to steel and other metals. This is due to the fact that it uses significantly less energy to be produced, consumes significantly less fossil fuels, and has a significantly lower total environmental impact. Glass is easily found in nature and does not require complex extraction methods, thus it does not discharge significant amounts of contaminated water into nature [15].

Because the manufacture of glass fibers is less complex and dangerous than that of steel, it takes at least 75% less energy than that of steel and other metals. Furthermore, with a specific weight of 1.9 kg/dm3 compared to 7.85 kg/dm3 for steel, it consumes more than half the energy required for transportation. Elements that are detrimental to health or the environment are rarely discharged during the manufacturing process since pultrusion occurs in a completely contained environment, reducing the creation of volatile compounds to a bare minimum. The resin used to make GFRP is generated from a byproduct of processed crude oil [15].

In adverse conditions, GFRP bars have a service life of more than 50 years on average. Another attribute that makes this material more environmentally friendly and sustainable is that it does not require any conservation treatments such as galvanizing or other anti-oxidation treatments.
After its useful life, GFRP is completely recyclable and can be used in a variety of fields. Additionally, treated GRP waste is a high-quality option for the cement industry, where it is used as both a fuel and a mineral raw material (SiO_2) [15].

Even though recycling is more difficult due to the material value, being glass an order of magnitude less than carbon fibers, there are various potential avenues for glass reinforced polymer (GRP) waste:

- Cement kiln processing: Composite waste can be co-processed as solid recovered fuel (SRF) in cement kilns with other wastes. This recovers energy from the organic portion, and mineral fillers and glass are converted into cement clinker feedstock [16];

- GRP can be delivered to energy from waste (EfW) plants for incineration. The organic component is used to recover energy. Bottom ash from incinerators can be turned into aggregates or utilized in building, however in certain circumstances it is still landfilled [16];

- Mechanical recycling to fine filler: GRP can be crushed to a fine filler. However, it is not often cost effective since the energy input required to grind to a filler that replaces a low-value product such as calcium carbonate is inadequate [16];

- Mechanical recycling with fiber retention: GRP can be ground to a reduced extent, leaving bundles of reinforcing fibres. This saves energy while producing a more valuable product than fine filler [16].

1.6 Research significance and limitations

There is a need of an alternative sustainable material to replace the conventional steel bar used to reinforce the concrete, for the several reasons discussed here above and specially for the structures to be made in certain environments. Although alternatives exist and are made in bars to be used as internal reinforcement, they are not used since the design techniques are not well known, and very little research has been done on bars as armor.

In this study an empirical formula is derived to calculate the resisting moment in case of GFRP reinforced beams, which can be used to calculate the minimum reinforcement, for this purpose further studies are required for instance to find statistically the depth of the neutral axis in case of GFRP reinforced beams. Furthermore, to get an appropriate validation, some beams should be designed by using this formula and eventually cast and tested.

Since GFRP reinforced beams doesn't show a ductile behaviour, these shouldn't be used where ductility is required for instance in seismic zones.

1.7 Method

This thesis work is a qualitative study where data was obtained from the literature. In particular, the publications listed in the chapter 2 were analyzed. It has been done in the following steps: Literature survey, literature study and analysis of the data retrieved from these articles. The data used was regarding the flexural behavior of concrete beams reinforced with GFRP, which was studied in these articles by mean of laboratory testing.

With the data retrieved (bending test results, specimens details, materials properties etc.) a numerical simulation is performed using moment-curvature relationship, using stress-strain laws ($\sigma - \epsilon$).

Obtained relations are then validated through comparison with the experimental data.

Chapter 2

Flexural behaviour of GFRP reinforced beams

Flexural behaviour of GFRP reinforced beams was investigated by reviewing the following publications:

- Evaluation of the flexural strength and serviceability of concrete beams reinforced with different types of GFRP bars. [17];
- Experimental response and code models of GFRP R.C. beams in bending [18];
- Performance of concrete beams reinforced with GFRP bars under monotonic loading [19];
- Flexural strength and serviceability of GFRP-Reinforced lightweight self-consolidating concrete beams [20];

- Flexural performance of concrete beams reinforced by GFRP bars and strengthened by cfrp sheets [21];
- Performance of concrete beams partially/ fully reinforced with glass fiber polymer bars [22];
- Performance of concrete beams reinforced with GFRP Bars [23].

2.1 Tests on GFRP beams

All of these papers were about GFRP reinforced full scale beams with varying reinforcement ratios. In all of these papers, beams were subjected to four-point bending tests. There were some beams in these articles reinforced with hybrid reinforcement, which were neglected.

2.1.1 El-Nemr et. al.

El-Nemr et al. [17] investigated the flexural behavior and serviceability of concrete beams reinforced with GFRP bars of varying elasticity modulus and surface profiles. They tested 17 full-scale beams using four point bending test til failure. They've designed over reinforced beams, to have the failure in compression. They reinforced the beams with three types of GFRP bars, shown in the figure 2.1, their properties are reported in the table 2.1.

Figure 2.1: Types of reinforcing bars [17]

Bar type	Diameter (mm)	ffu (MPa)	Ef (GPa)	εu (%)	fn (MPa)
GFRP-1	13	817 ± 9	48.7 ± 0.6	1.7	790
	15	751 ± 23	48.1 ± 1.6	1.6	683
	20	728 ± 24	47.6 ± 1.7	1.5	656
	22	693 ± 23	46.4 ± 1.5	1.5	625
	25	666 ± 74	53.2 ± 2.1	1.3	444
GFRP-2	13	1639 ± 61	67.0 ± 1.0	2.5	1456
	15	1362 ± 33	69.3 ± 3.2	2.0	1263
	20	1082 ± 37	52.5 ± 1.7	2.1	971
	25	1132 ± 23	66.3 ± 0.9	1.7	1063
GFRP-3	15	1245 ± 45	59.5± 1.1	2.1	1110
	25	906 ± 29	60.3 ± 2.9	1.5	819

ffu : Tensile Strength (average ± Standard deviation)
Ef : Elasticity Modulus (average ± Standard deviation)
εu : Ultimate Strain
fn : Guaranteed Tensile Strength

Table 2.1: GFRP properties, El-Nemr [17]

The properties of the beam they have cast is stated in the tables 2.2 2.3 and , their geometry is shown in the figure 2.2.

Series	Beam	*fc' (MPa)*	*ft (MPa)*	ρ f (%)	ρ fb (%)
I	*3#13G1*	33.50	3.60	0.56	0.43
	5#13G1	38.95	3.81	0.91	0.59
	2#13G2	33.50	3.60	0.38	0.15
III	*3#15G1*	38.95	3.81	0.84	0.65
	4#15G1	38.95	3.81	1.12	0.65
	2#15G2	29.00	2.50	0.56	0.20
	2#15G3	33.83	3.11	0.56	0.21
III	*6#15G1*	33.50	3.60	1.82	0.50
	5#15G2	29.00	2.50	1.52	0.20
	5#15G3	33.80	3.10	1.52	0.23
IV	*2#20G1*	38.95	3.81	0.81	0.69
	3#20G1	42.10	3.18	1.21	0.73
	2#22G1	38.95	3.81	1.08	0.61
	3#20G2	48.13	3.96	1.21	0.34
V	*2#25G1*	48.13	3.96	1.46	0.83
	2#25G2	48.13	3.96	1.46	0.38
	2#25G3	33.80	3.10	1.51	0.42

Table 2.2: Test specimens details 1, El-Nemr et. al. [17]

Series	Beam	ρ f/ρ fb	*Af Ef (kN)*	Reinforcement configuration
I	*3#13G1*	1.31	18,347	3 No. 13 – 1 row
	5#13G1	1.54	29,864	5 No. 13 – 1 row
	2#13G2	2.45	17,286	2 No. 13 – 1 row
III	*3#15G1*	1.30	28,716	3 No. 15 – 1 row
	4#15G1	1.73	38,288	4 No. 15 – 1 row
	2#15G2	2.79	27,581	2 No. 15 – 1 row
	2#15G3	2.69	23,681	2 No. 15 – 1 row
III	*6#15G1*	3.67	59,7	6 No. 15 – 2 rows
	5#15G2	7.58	68,954	5 No. 15 – 2 rows
	5#15G3	6.47	59,203	5 No. 15 – 2 rows
IV	*2#20G1*	1.61	27,037	2 No. 20 – 1 row
	3#20G1	1.67	40,555	3 No. 20 – 1 row
	2#22G1	1.76	35,264	2 No. 22 – 1 row
	3#20G2	3.59	44,73	3 No. 20 – 1 row
V	*2#25G1*	1.75	54,264	2 No. 25 – 1 row
	2#25G2	3.85	67,626	2 No. 25 – 1 row
	2#25G3	3.57	61,506	2 No. 25 – 1 row

Table 2.3: Test specimens details El-Nemr et. al. [17]

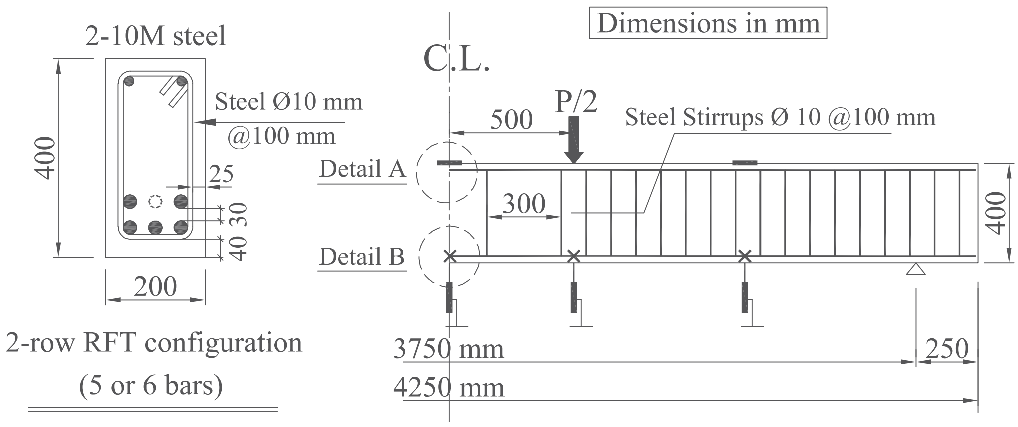

Figure 2.2: Beams geometry, El-Nemr et. al. [17]

Series	Beam	*Mcr (kN.m)*	*Mn (kN.m)*	Failure mode
I	*3#13G1*	13.46	81.34	C.C.
	5#13G1	15.26	130.6	C.C.
	2#13G2	13.75	82.78	C.C.
III	*3#15G1*	12.21	101.3	C.C.
	4#15G1	15.61	138.2	C.C.
	2#15G2	11.22	95.93	C.C.
	2#15G3	10.92	91.31	C.C.
III	*6#15G1*	11.98	118.3	C.C.
	5#15G2	12.2	129.3	C.C.
	5#15G3	12.61	110.6	C.C.
IV	*2#20G1*	15.36	107.4	C.C.
	3#20G1	16.32	140.4	C.C.
	2#22G1	12.88	132.3	C.C.
	3#20G2	12.29	171.4	C.C.
V	*2#25G1*	11.32	161.7	C.C.
	2#25G2	16.77	167.2	C.C.
	2#25G3	13.2	115.9	C.C.

Table 2.4: Cracking and Ultimate Moments, El-Nemr et. al, [17]

The test results they've obtained are shown in the table 2.4, which are also plotted in the figures 2.3 and 2.4.

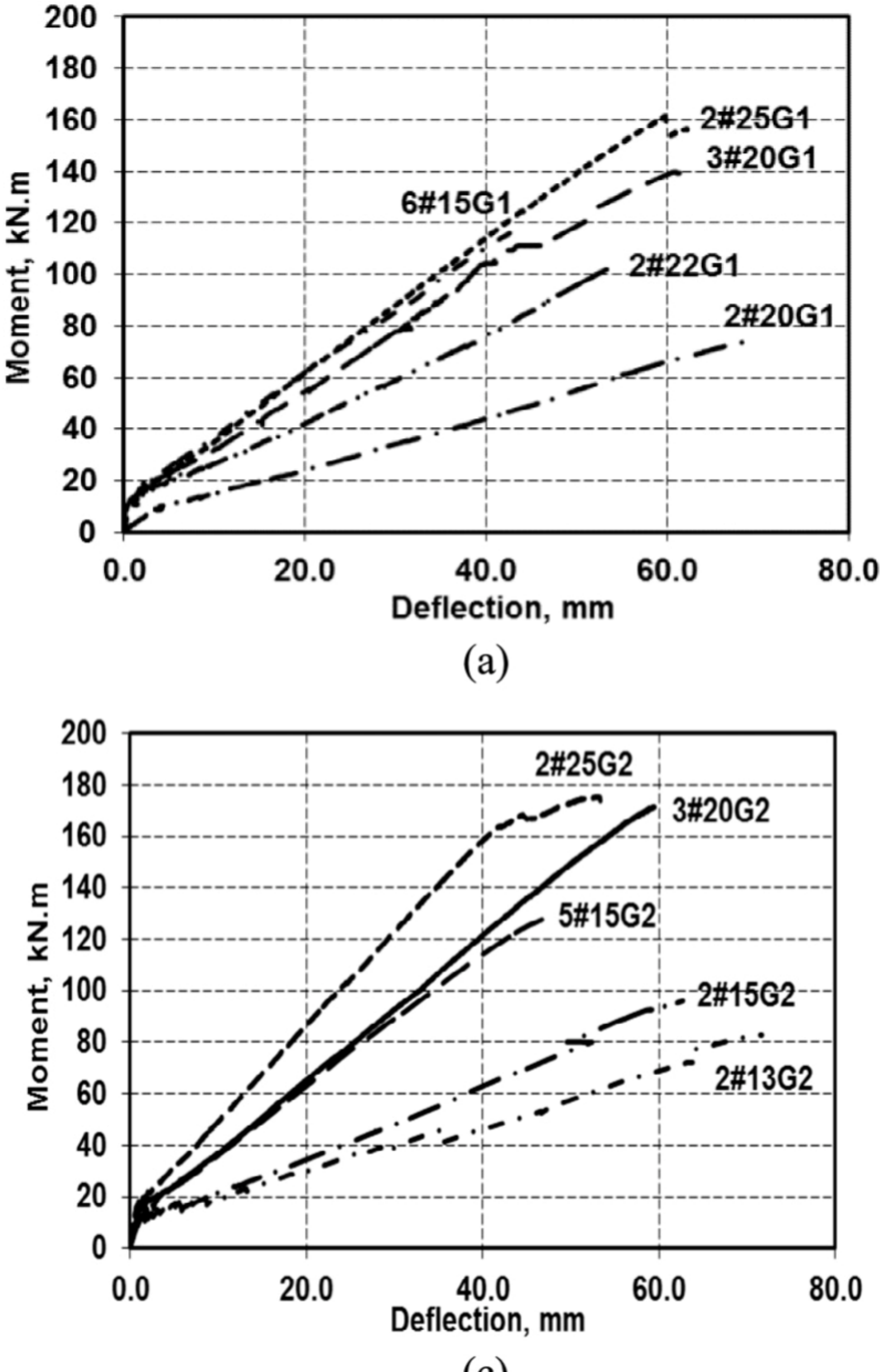

Figure 2.3: Deflection vs. applied moment plot 1, El-Nemr et. al. [17]

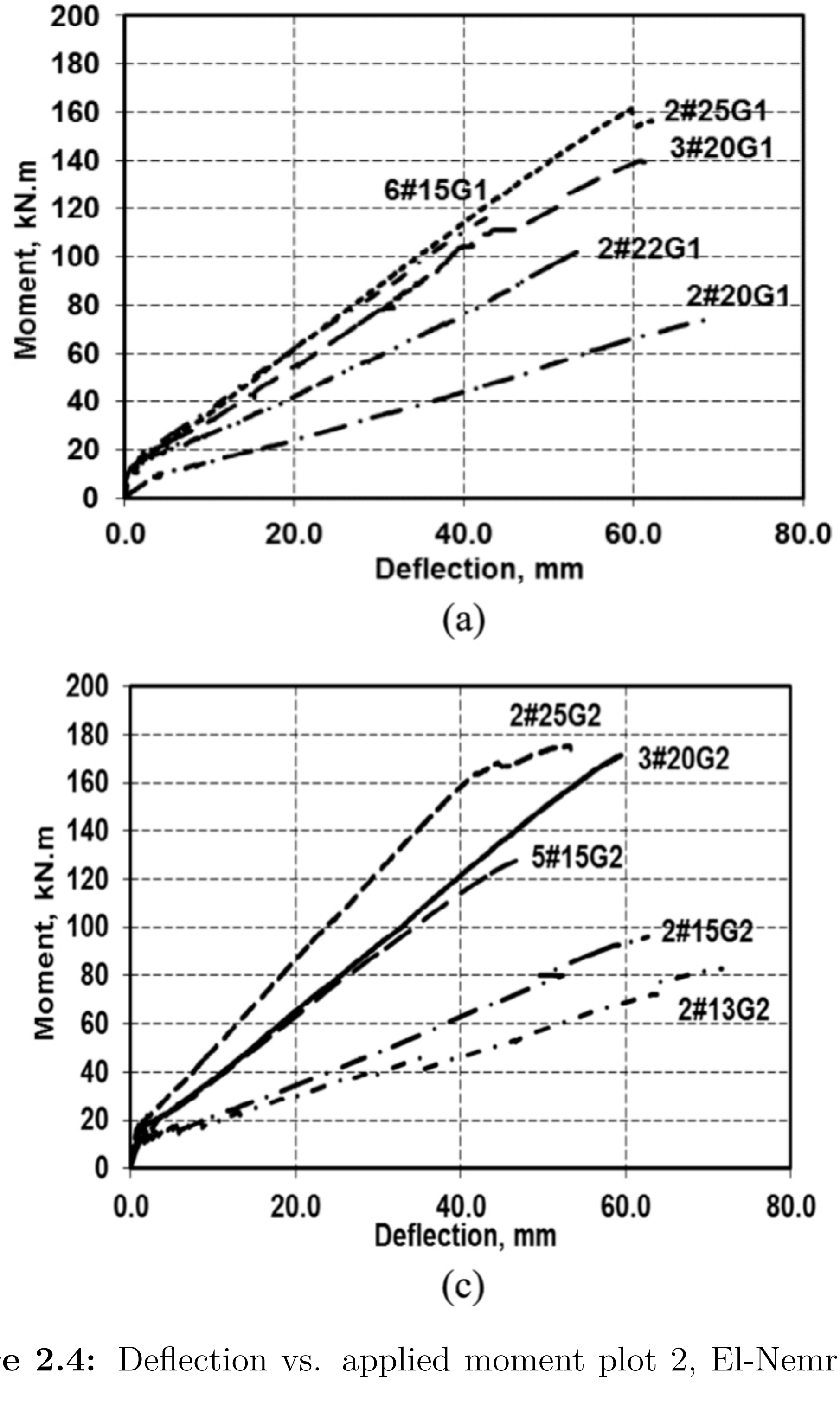

Figure 2.4: Deflection vs. applied moment plot 2, El-Nemr et. al. [17]

2.1.2 M. Pecce et. al.

M. pecce et. al. [18] similarly tested 3 beams. Their geometry is reported in the figure 2.5. The concrete they've used for all the 3 beams had a compression strength of 30 MPa. The bars they've used had actual average tensile strength of 600 MPa and longitudinal elasticity modulus of 42 GPa. The results they have obtained are shown in the figure 2.5.[18]

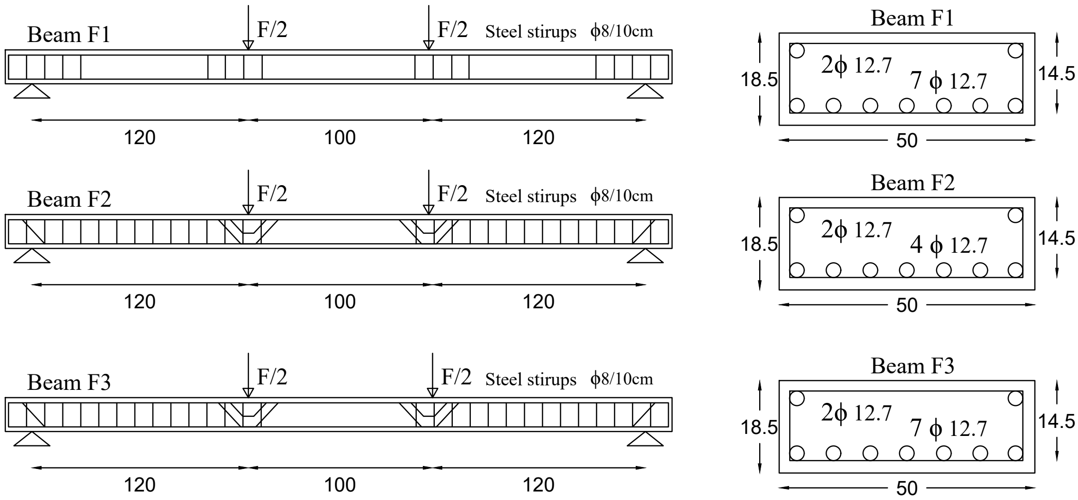

Figure 2.5: Beams geometry, M. Pecce et. al. [18]

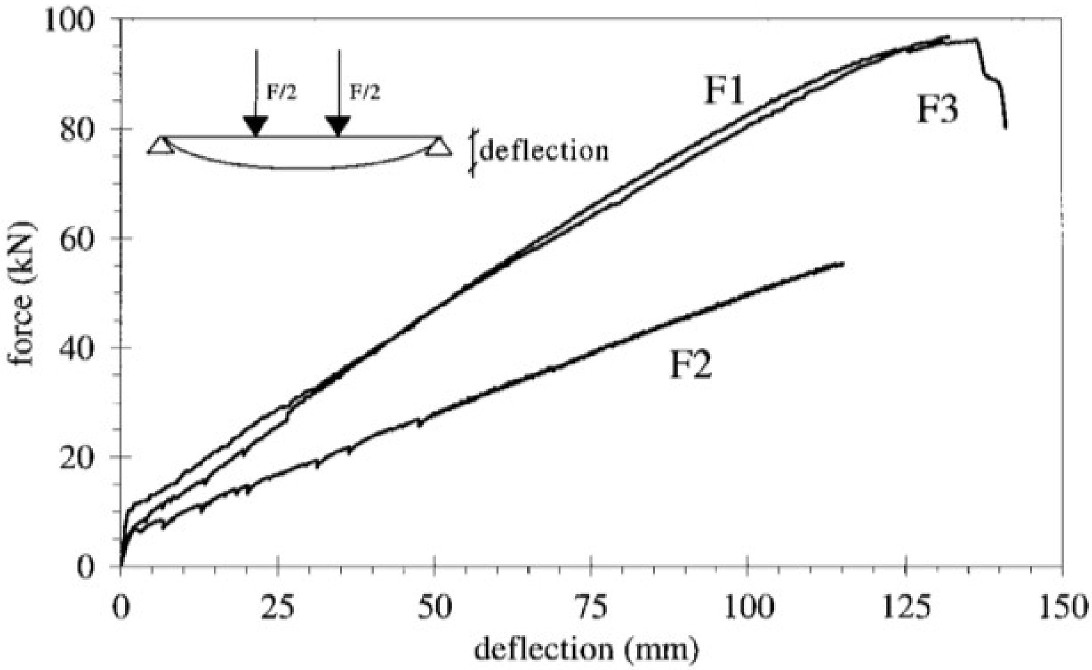

Figure 2.6: Test results, M. Pecce et. al. [18]

2.1.3 A. Ramachandra Murthy et. al.

A.Ramachandra Murthy et. al. [19] tested eleven beams, out of which 3 were reinforced with 10 mm GFRP bars and 2 with 13 mm GFRP bars, while the others were reinforced with steel and they compared the average behaviour of GFRP reinforced beams with the relative diameter steel reinforced beams[19]. Specimens geometry is shown in the figure 2.7. Specimens details is shown in the tables 2.5 and 2.6. For our research, the average data of beams reinforced with 13 mm GFRP were considered. Load deflection curves for 13 mm diameter GFRP reinforced beams are shown in the figure 2.8.Meanwhile, comparison between the load deflection curves of the four type beams is shown in the figure 2.9

Specimen ID	Crack initiation load (kN)	Ultimate load (kN)	Deflection at ultimate load (mm)
GFRP-1S-10	12.1	53	14.8
GFRP-2S-10	12.0	58	16.0
GFRP-3S-10	10.1	61	16.1
GFRP-4S-13	14.0	80	20.3
GFRP-5S-13	12.0	90	21.9
TMT-1S-10	22.0	69	17.8
TMT-2S-10	18.0	56	14.8
TMT-3S-10	20.0	54	22.7
TMT-1S-12	15.9	98	12.4
TMT-2S-12	24.0	94	11.0
TMT-3S-12	20.6	97	9.16

Table 2.5: Test specimens details, A. Ramachandra M. et. al. [19]

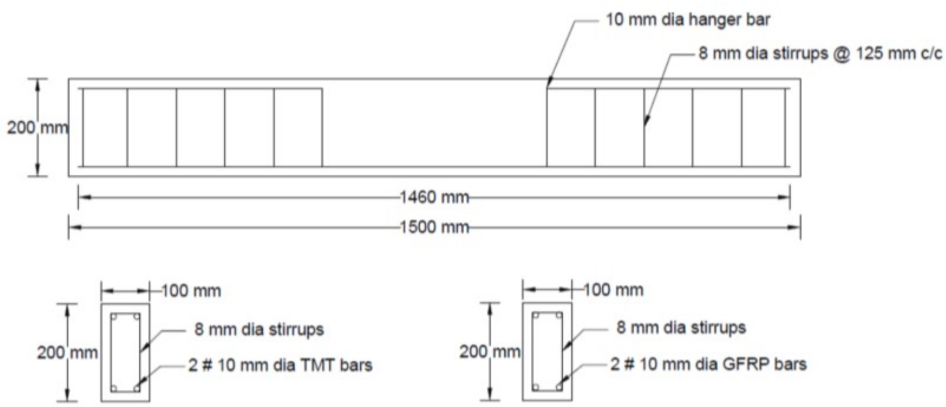

Figure 2.7: Beams geometry, Ramachandra et. al. [19]

Specimen ID	Average crack initiation load (kN)	Average ultimate load (kN)	Average deflection at ultimate load (mm)
GFRP-1S-10 GFRP-2S-10 GFRP-3S-10	11.4	57.3	15.6
GFRP-4S-13 GFRP-5S-13	13.0	85.0	21.5
TMT-1S-10 TMT-2S-10 TMT-3S-10	20.0	59.7	18.5
TMT-1S-12 TMT-2S-12 TMT-3S-12	20.1	96.3	10.8

Table 2.6: Test specimens details, average values A. Ramachandra M. et. al. [19]

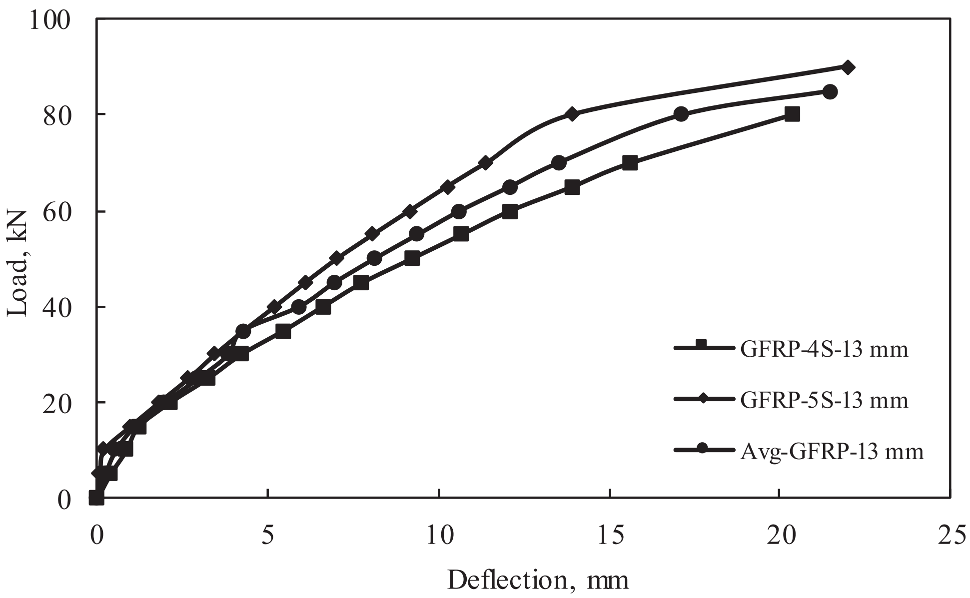

Figure 2.8: Load deflection curves GFRP 13 mm reinforced beams, Ramachandra et. al. [19]

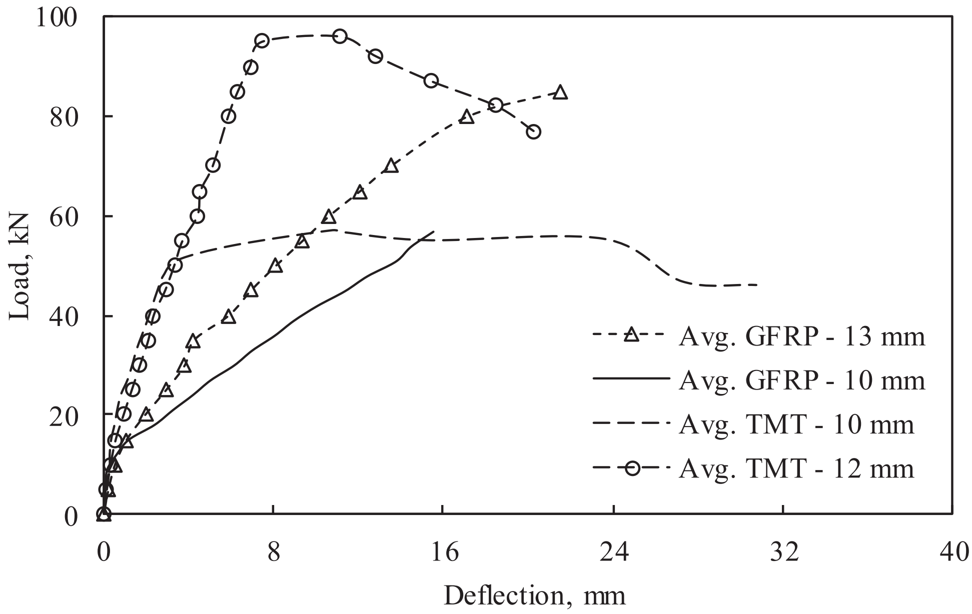

Figure 2.9: Average load deflection curves, Ramachandra et. al. [19]

2.1.4 Sehab Mehany et. al.

For this paper, ten beams were tested, with four point bending test. Eight beams of these were Light weight self-consolidating concrete (LWSCC) beams, seven reinforced with GFRP and one with steel. Two of the beams were made of Normal-Weight Concrete (NWC), reinforced with GFRP bars. Two different types of bars were employed as shown in the figure 2.10. Properties of the bars are shown in tables 2.7 and 2.8.

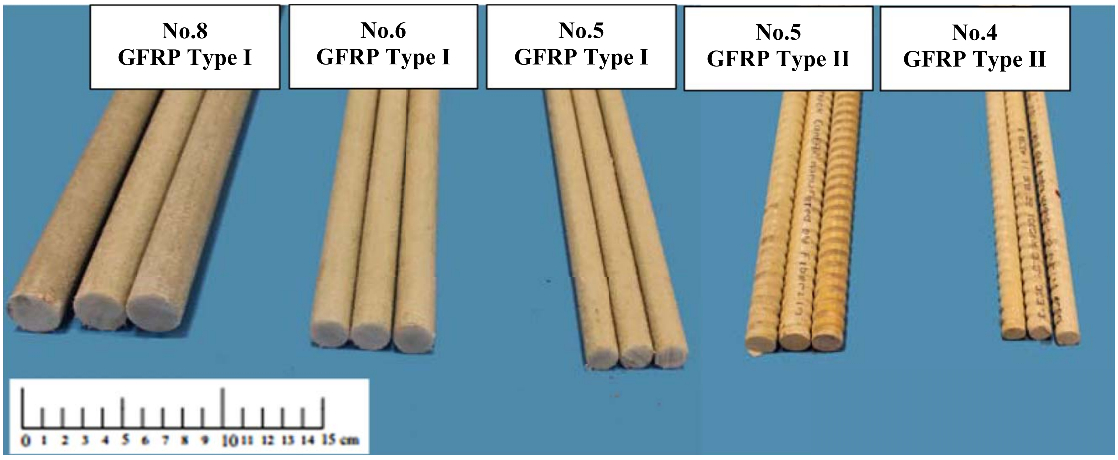

Figure 2.10: Types of reinforcing bars, Sehab Mehany et. al. [20]

RFT type	Bar size	Surface configuration	d_b (mm)	A_f (mm²)
GFRP bars—Type I	No. 8	Sand-coated	25.4	510
	No. 6		19.1	285
	No. 5		15.9	199
GFRP bars—Type II	No. 5	Helically grooved	15.9	199
	No. 4		12.7	129
Steel bars	15M	Ribbed	16.0	200

Table 2.7: GFRP properties 1, Shehab Mehany et. al. [20]

RFT type	A_{im} (mm²)	E_f (GPa)	f_{fu} (MPa)	ε_{fu} (%)
GFRP bars—Type I	557	64.5	1175	1.82
	325	64.2	1382	2.15
	229	65.3	1451	2.22
GFRP bars—Type II	221	59.5	1245	2.09
	151	58.3	1170	2.01
Steel bars	—	200	$f_y = 450$	$\varepsilon_y = 0.2$

Table 2.8: GFRP properties 2, Shehab Mehany et. al. [20]

The tested specimens are shown in the figure 2.11 and their properties are reported in the table 2.9. The test results are reported in the table 2.10, Moment deflection curves are plotted in the figure 2.12.

Beam ID	Reinforcing material	f'_c (MPa)	Concrete tensile strength (MPa)	Flexural reinforcement	
				Reinforcement configuration	ρ_f (%)
LS-GI-3#8	GFRP Type I	43.0	2.95	3#8—1 layer	3.22
LS-GI-4#6	GFRP Type I	43.0	3.05	4#6—2 layers	2.52
LS-GI-3#6	GFRP Type I	43.8	3.05	3#6—1 layer	1.78
LS-GI-3#5	GFRP Type I	43.8	3.05	3#5—1 layer	1.18
LS-GI-2#5	GFRP Type I	43.8	3.05	2#5—1 layer	0.78
LS-GII-3#5	GFRP Type II	43.0	2.95	3#5—1 layer	1.18
LS-GII-2#5	GFRP Type II	43.0	2.95	2#5—1 layer	0.78
LS-S-3#15M	Steel	43.8	3.05	3#15M—1 layer	1.18
N-GI-3#8	GFRP Type I	41.3	3.6	3#8—1 layer	3.22
N-GI-3#5	GFRP Type I	41.3	3.6	3#5—1 layer	1.18

Table 2.9: Specimens details , Sehab Mehany et. al. [20]

Beam ID	Reinforcing material	Failure mode	Mcr-exp (kN · m)	Mn-exp (kN · m)
LS-GI-3#8	GFRP Type I	CC	10.5	106.5
LS-GI-4#6	GFRP Type I	CC	9.5	85.5
LS-GI-3#6	GFRP Type I	CC	8.0	89.0
LS-GI-3#5	GFRP Type I	CC	9.0	81.0
LS-GI-2#5	GFRP Type I	CC	8.5	67.5
LS-GII-3#5	GFRP Type II	CC	8.0	78.0
LS-GII-2#5	GFRP Type II	CC	7.0	65.5
LS-S-3#15M	Steel	SY+ CC	9.5	58.5
N-GI-3#8	GFRP Type I	CC	12.0	104.5
N-GI-3#5	GFRP Type I	CC	11.0	81.5

Table 2.10: Test results, Sehab Mehany et. al. [20]

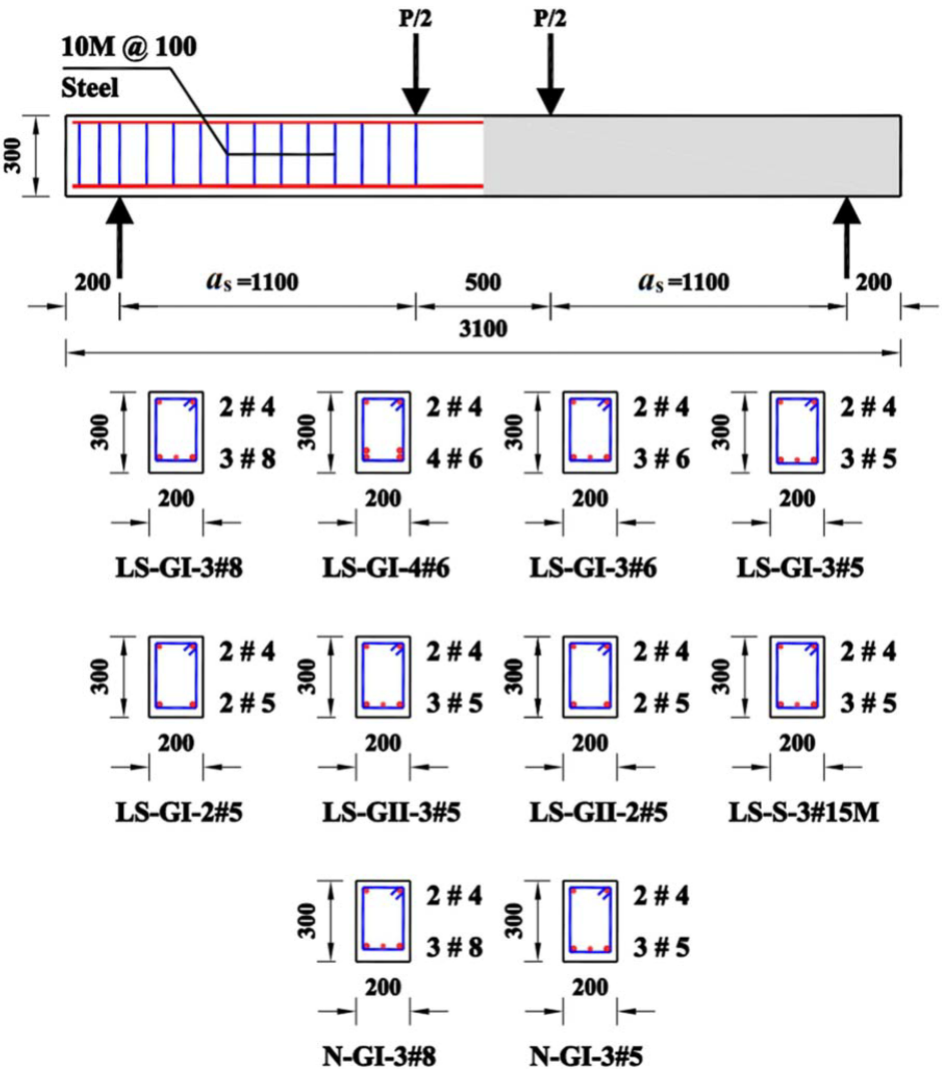

Figure 2.11: Specimens Geometry , Sehab Mehany et. al. [20]

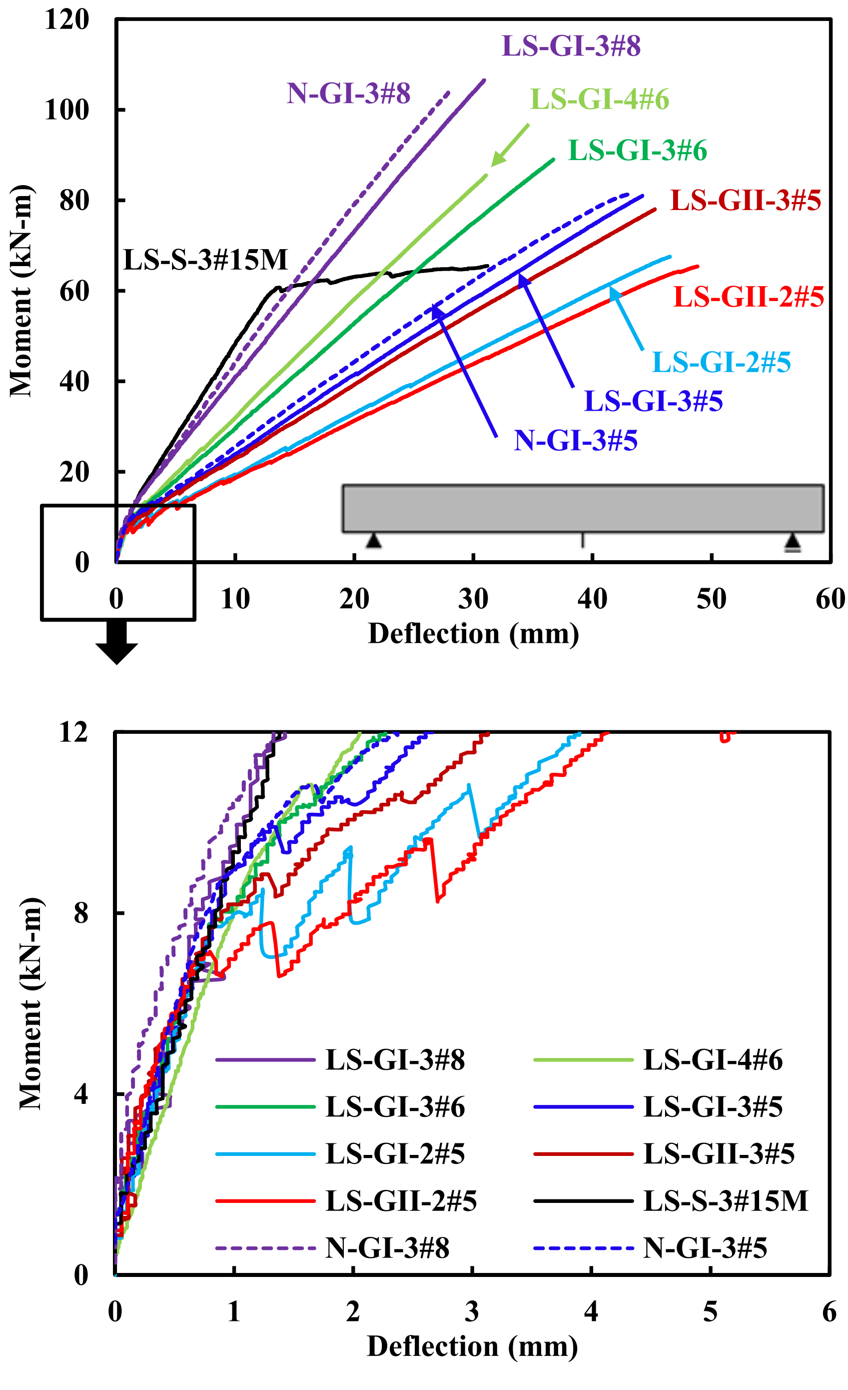

Figure 2.12: Moment deflection curves, Sehab Mehany et. al. [20]

2.1.5 H. Falah Hassan et. al.

H. Falah Hassan et. al. [21] tested beams reinforced with the GFRP bars and strengthened with CFRP sheets in the tensional zone up to failure [21]. Only GFRP-reinforced beams were considered for this investigation. Therefor, only beams B2-0C and B3-0C were considered, both beams were reinforced with 14 mm GFRP bars, with 2 and 3 bars as bottom reinforcement respectively. Specimens geometry is shown in the figure 2.13, bar specifications are shown in the table 2.11 specimens properties are shown in the table 2.12. The test results of the two beams of our interest are displayed in the figure 2.14.

Bar type	GFRP
Nominal diameter (mm)	14
Ultimate strength (MPa)	1200
Modulus of elasticity (MPa)	55000
Strain$\varepsilon u(\mu\varepsilon)$	1950

Table 2.11: GFRP bars specifications

Beam Series	Beam specimen	Beam dimensions Width (mm)	Depth (mm)	Reinforcement Bottom	Top	No. Of CFRP layers
0c	B2—0C	150	200	2 ϕ 14 mm	2 ϕ 4mm	0
	B3—0C	150	200	3 ϕ 14 mm	2 ϕ 4mm	0
1c	B2—1C	150	200	2 ϕ 14 mm	2 ϕ 4mm	1
	B3—1C	150	200	3 ϕ 14 mm	2 ϕ 4mm	1
	B4—1C	150	200	4 ϕ 14 mm	2 ϕ 4mm	1
	B5—1C	150	200	5 ϕ 14 mm	2 ϕ 4mm	1
2c	B2—2C	150	200	2 ϕ 14 mm	2 ϕ 4mm	2
	B3—2C	150	200	3 ϕ 14 mm	2 ϕ 4mm	2
	B4—2C	150	200	4 ϕ 14 mm	2 ϕ 4mm	2
	B5—2C	150	200	5 ϕ 14 mm	2 ϕ 4mm	2

Steel stirrups : ϕ 8@75cm
Concrete compressive strength $fc = 35$ MPa
Effective span length : 1500 mm

Table 2.12: Specimens details, H. Falah Hassan et. al.[21]

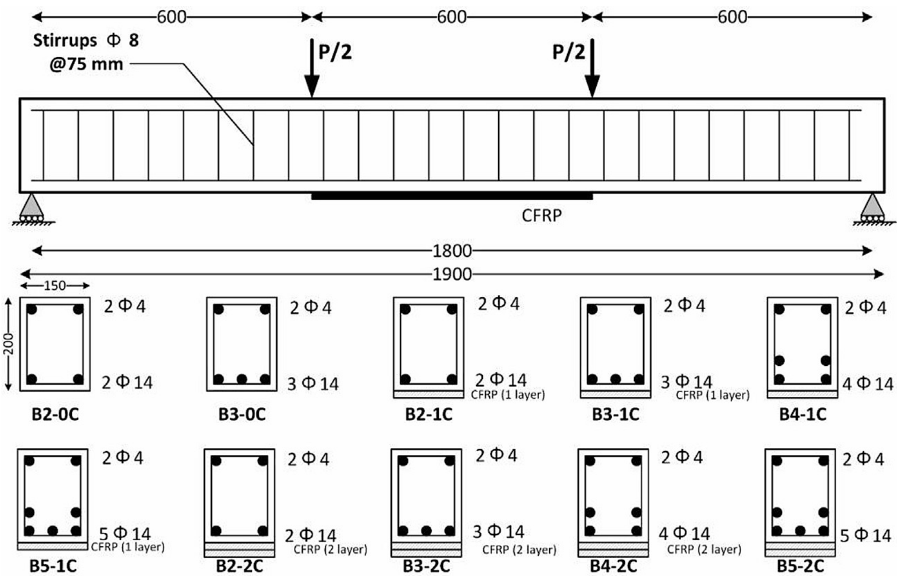

Fig. 1. Tested beams geometry and details.

Figure 2.13: Beams geometry, H. Falah H. et. al. [21]

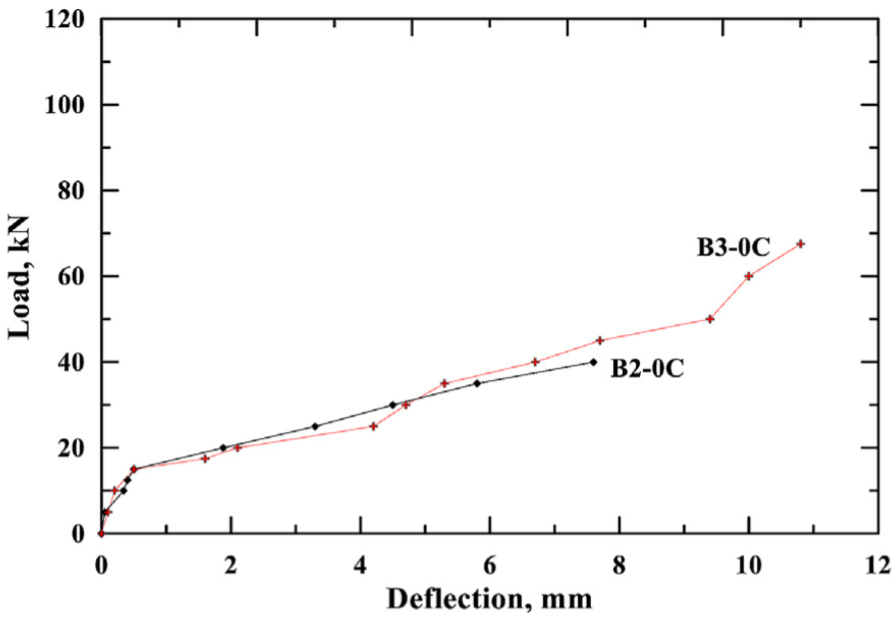

Figure 2.14: Load deflection curve, H. Falah H. et. al. [21]

2.1.6 Mohamed S. Moawad & Ahmad Fawzi

For this paper the authors tested six beams cast with two different concrete mixtures to achieve characteristic compressive strength of 30 MPa and 60 Mpa. Two of these beams featured simply GFRP reinforcement, whereas the rest were entirely steel reinforced or had hybrid reinforcement. [22]. Beams geometry is shown in the figure 2.15. Beams reinforcement detail is shown in the figure 2.13. Test results are shown in the table 2.14 and the table 2.15. Load-deflection curves plot is shown in the figure 2.16.

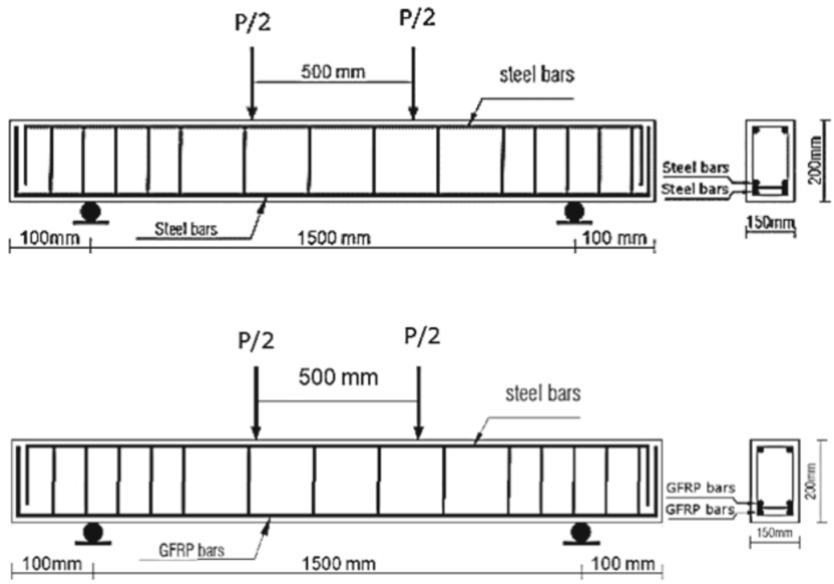

Figure 2.15: Beams geometry, M. S. Moawad, A. Fawzi [22]

Group no.	Beam ID	Reinforcement		Steel stirrups
		Bottom	Top	
Group 1	B1	4T10 steel bars	2R8 steel bars	6 ϕ 8
	B2	4 ϕ 10 GFRP bars	2 ϕ 8 GFRP bars	6 ϕ 8
	B3	2 ϕ 10 GFRP bars + 2T10 steel bars	2R8 steel bars	6 ϕ 8
Group 2	B4	4T10 steel bars	2R8 steel bars	6 ϕ 8
	B5	4 ϕ 10 GFRP bars	2 ϕ 8 GFRP bars	6 ϕ 8
	B6	2 ϕ 10 GFRP bars + 2T10 steel bars	2R8 steel bars	6 ϕ 8

Table 2.13: Specimens details, M. S. Moawad, A. Fawzi [22]

Beam ID	Pcr (ton)	Δ cr (mm)	Pv (ton)	Δ y (mm)	Pu (ton)	Δ u (mm)	Failure Mode	Failure Type
B1	3.50	4158	7.98	10.40	9.8	26.87	Shear failure	C.C.
B2	1.80	1.60	—	—	10.96	33.90	Flexure failure	GFRP
B3	1.87	1.24	7.10	9.50	10.28	39.20	Flexure failure	GFRP
B4	4.75	4.62	10.95	11.56	12.16	23.93	Shear failure	C.C.
B5	1.80	0.68	—	—	14.22	32.40	Flexure failure	GFRP
B6	1.88	2.91	8.76	14.58	13.12	34.05	Shear failure	GFRP

Table 2.14: Tests results, M. S. Moawad, A. Fawzi [22]

Beam	Dimensions (mm)		fcu	Test results		
ID	width, b	height, h	(Mpa)	Pu (kN)	Δ max (mm)	Pcr (kN)
B1	150	200	346	97.1	27.12	22
B2	150	200	351	109.6	33.68	12
B3	150	200	338	102.8	41.54	18
B4	150	200	630	121.6	26.15	25
B5	150	200	652	142.2	32.4	18
B6	150	200	655	131.2	34.05	22

fcu : actual compressive strength concrete beams
Pu : ultimate load
Pcr : initial cracking load
Δ max : maximum deflection at midspan

Table 2.15: Load deflection, M. S. Moawad, A. Fawzi [22]

Only flexuraly failed beams were considered.

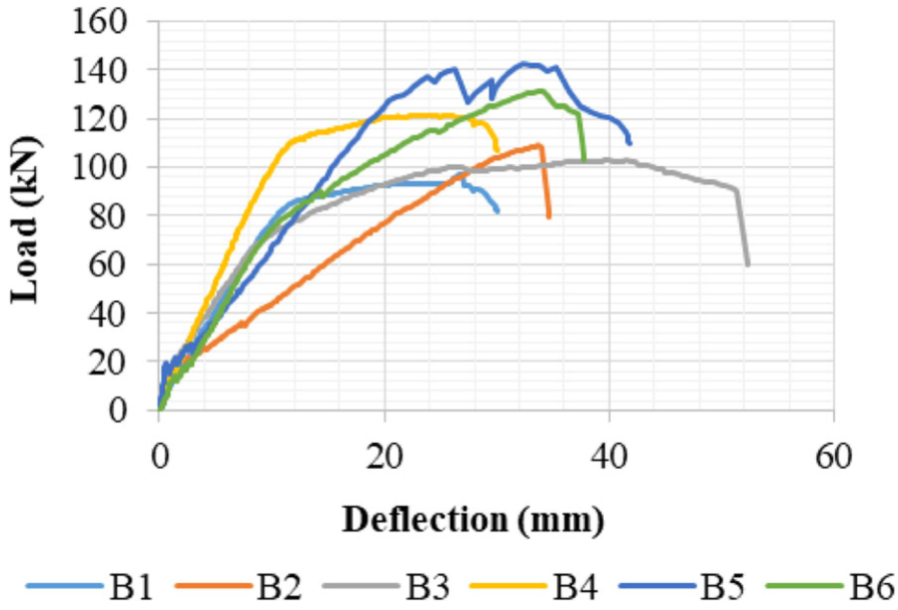

Figure 2.16: Load-deflection curves, M. S. Moawad, A. Fawzi [22]

2.1.7 Sungwoo Shin et. al.

Sungwoo Shin et. al. [23] tested twelve beams, five of which were reinforced with GFRP, one with steel and the rest with hybrid reinforcement. The beams geometry is shown in the figure 2.17, the reinforcement characteristics in the figure 2.16, specimen details are shown in the table 2.17, Test results are shown in the table 2.18. The load-deflection curves are plotted in the figure 2.18.

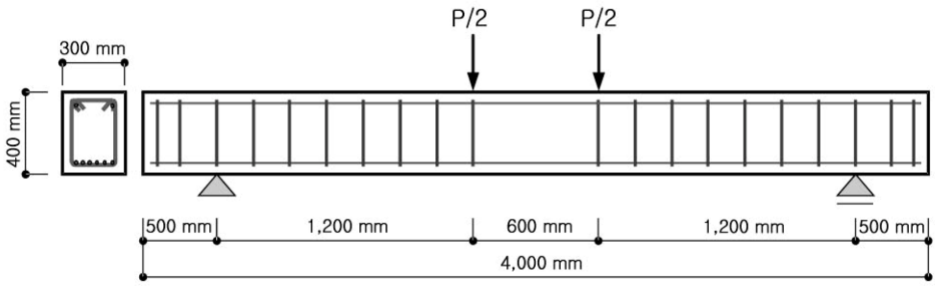

Figure 2.17: Beams Geometry, Sungwoo shin et. al. [23]

Reinforcement type	Diameter (mm)	Modulus of Elasticity (GPa)	Yielding strength (MPa)	Tensile Strength (MPa)
	10	200	460	560
Steel	16	200	410	540
	22	200	400	560
GFRP	13	41	-	690

Table 2.16: Reinforcement characteristics, Sungwoo Shin et.al. [23]

Specimens	Reinforcement type	f'c (Mpa)	ρ	ρ/ρ b	Overall depth h (mm)	Width b (mm)
SB-2	Steel	30	0.73	0.2	40	30
HSB-3		50	1.09	0.25		
FB-2	GFRP	30	0.24	0.46	40	30
FB-3			0.36	0.70		
FB-4			0.48	0.93		
FB-6			0.72	1.39		
FB-8			0.96	1.86		
HFB-3	Hybrid	50	0.36	0.57	40	30
HFB-4			0.48	0.76		
HFB-6			0.72	1.14		
HFB-8			0.96	1.51		
HFB-10			1.27	2.00		

Table 2.17: Specimens details, Sungwoo shin et. al. [23]

Specimens	ρ/ρ b	Pmax (kN)	δ max (mm)	Failure mode
SB-2	0.2	256.6	44.5	Flexural failure
HSB-3	0.25	340.7	47.8	Flexural failure
FB-2	0.46	114.9	39.8	FRP rupture
FB-3	0.70	185.3	45.3	FRP rupture
FB-4	0.93	209.8	56.1	FRP rupture
FB-6	1.39	285.9	53.3	Concrete crushing
FB-8	1.86	371.0	63.0	Concrete crushing
HFB-3	0.57	155.4	40.2	FRP rupture
HFB-4	0.76	198.4	45.2	FRP rupture
HFB-6	1.14	334.1	54.2	FRP rupture/Bond failure
HFB-8	1.51	363.4	56.8	Concrete crushing
HFB-10	2.00	365.6	43.0	Concrete crushing

Table 2.18: Load and deflection,Sungwoo shin et. al. [23]

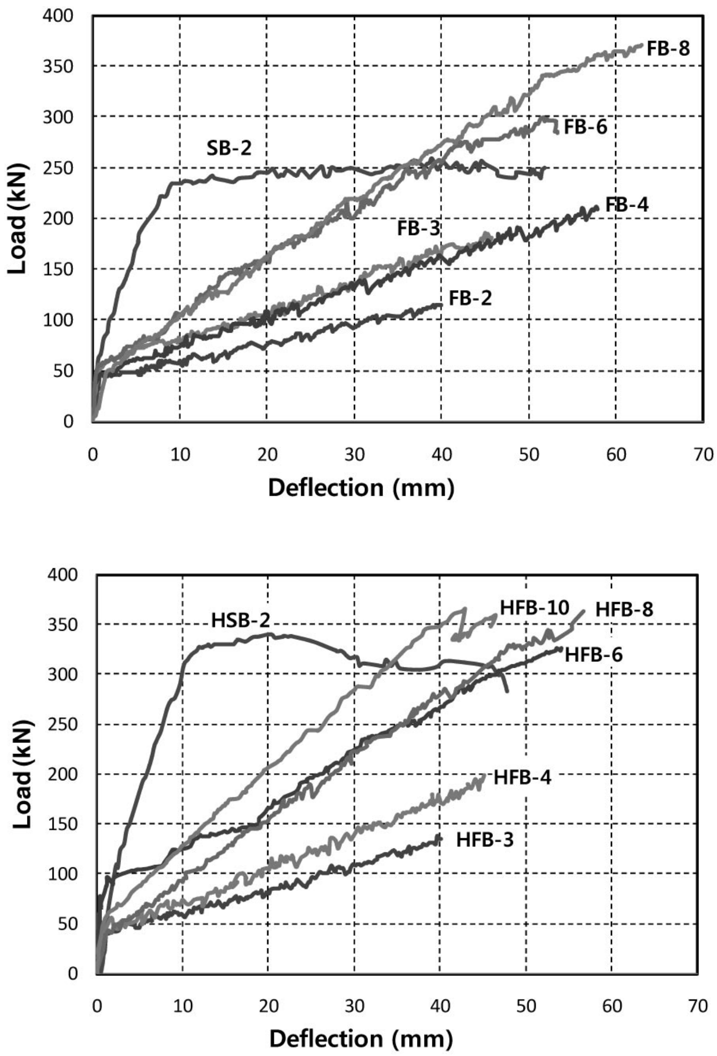

Figure 2.18: Loaad-deflection curves, Sungwoo shin et. al. [23]

2.2 Summary and conclusions

The data collected from these articles are summarized in the table 2.19 the ultimate moment (Mu, exp) is calculated where it is not provided, using the beams loading configuration and loading forces values at failure.

- The typical GFRP reinforced concrete beams load deflection behaviour is bi-linear, it has a linear branch till the appearance of the first crack, than another nearly linear branch follows till failure.

- The GFRP reinforced beams are less stiffer than steel reinforced beams, see figure 2.9 After the crack initiation, the stiffness of the GFRP reinforced beams is lowered even more [23].

- The deflection in GFRP reinforced beams is greater than steel reinforced beams. This is due to lower elasticity modulus of GFRP. To ensure enough flexural stiffness GFRP beams should be over-reinforced [23].

- If the beam is over-reinforced a pseudo-ductility can develop due to the non-linear behaviour of concrete in the post-peak branch, thus, the design is favorable if concrete failure is provided [18].

- The reinforcing ratio has no effect on the pre-cracking response of GFRP reinforced beams because it is governed by the gross concrete section [20].

Unlike steel reinforced concrete structures, where steel provide ductile behaviour, it is preferable to have concrete crushing [18]. **Both, the reinforcement failure and the concrete crushing are brittle type failures therefor, ductility design could not be adopted for GFRP reinforced beams.**

Article		Specimens denomination	N.b.	Diameter (mm)	Mu exp (kN . m)	Failure type	f'c (MPa)	fu (MPa)	h (m)	b (m)
Sehab Mehany et. al.		GI 4#6	4	19.1	85.61	CC	43	1382	0.3	0.2
		GI 3#6	3	19.1	89.04	CC	43.8	1382		
		GI 3#5	3	15.9	81.36	CC	43.8	1451		
		GI 2#5	2	15.9	67.83	CC	43.8	1451		
		GII 3#5	3	15.9	78.59	CC	43	1245		
		GII 2#5	2	15.9	65.67	CC	43	1245		
		N GI 3#5	3	15.9	81.72	CC	41.3	1451		
H. Falah Hassan et. al.		B2	2	14	23.81	GFRP	32	1200	0.2	0.15
		B3	3	14	40.36	GFRP	32	1200		
Mohamed S. M. & A. Fawzi		B2	4	10	27.40	GFRP	30	407	0.2	0.15
		B5	4	10	35.50	GFRP	60	407		
Sungwoo Shin et. al.		FB02	2	12.7	68.94	GFRP	30	690	0.4	0.3
		FB03	3	12.7	111.18	GFRP	30	690		
		FB04	4	12.7	125.88	GFRP	30	690		
		FB06	6	12.7	171.54	CC	30	690		
		FB08	8	12.7	222.60	CC	30	690		
El-Nemr et. al.	series 1	3 \# 13 G 1	3	13	80.30	CC	33.5	817	0.4	0.2
		5 \# 13 G 1	5	13	129.63	CC	38.95	817		
		2 \# 13 G 2	2	13	80.51	CC	33.5	1639		
	series 2	3 \# 15 G 1	3	15	71.44	CC	38.95	751		
		4 \# 15 G 1	4	15	138.22	CC	38.95	751		
		2 \# 15 G 2	2	15	94.26	CC	29	1362		
		2 \# 15 G 3	2	15	94.84	CC	33.83	1245		
	series 3	6 \# 15 G 1	6	15	115.21	CC	33.5	751		
		5 \# 15 G 2	5	15	125.84	CC	29	1362		
		5 \# 15 G 3	5	15	112.01	CC	33.8	1245		
	series 4	2 \# 20 G 1	2	20	71.90	CC	38.95	728		
		3 \# 20 G 1	3	20	139.21	CC	42.1	728		
		3 \# 20 G 2	2	22	169.17	CC	48.13	1082		
		2 \# 22 G 1	3	20	100.53	CC	38.95	693		
	series 5	2 \# 25 G 1	2	25	160.77	CC	48.13	666		
		2 \# 25 G 2	2	25	173.66	CC	48.13	1132		
		2 \# 25 G 3	2	25	107.93	CC	33.8	906		
M. Pecce et. al.		F2	4	12.7	57.71	GFRP	30	600	0.185	0.5
		F3	7	12.7	33.23	GFRP	30	600		
A. Ramachandra et. al.		GFRP-S-13	2	13	19.29	GFRP	40	673	0.2	0.1

N.b. = Number of bottom reinforcement bars
Mu. exp. = Experimental ultimate moment
f'c = Concrete compressive strength
fu = Ultimate tensile strength of the reinforcement

Table 2.19: Collected data summarized

Chapter 3

Parallel between GFRP reinforced concrete and steel reinforced concrete

In the steel reinforced concrete, depending on the amount of the reinforcement, the failure can be either brittle or ductile. In the figure 3.1 it is shown the behaviour of a beam, that undergoes three point bending test, with different reinforcement:

- In the case of plain concrete beam, $As = 0$, the ultimate load, Pu, is lower than the effective cracking load, $Pcr*$, therefor, the failure is very brittle.
- Reinforcement equal to the minimum amount is a limit condition, for which the ultimate load is equal to the cracking load, it is the case in which the ductility is equal to zero.
- Case in which the the reinforcement is greater than the minimum

amount $As > As, min$ the failure is ductile, the ultimate load is greater than the cracking load.

- Lastly, when the reinforcement is greater than the maximum reinforcement amount, the strength is way more higher but we have brittle type and sudden failure. This is because the compression resistance of the concrete is exceeded.

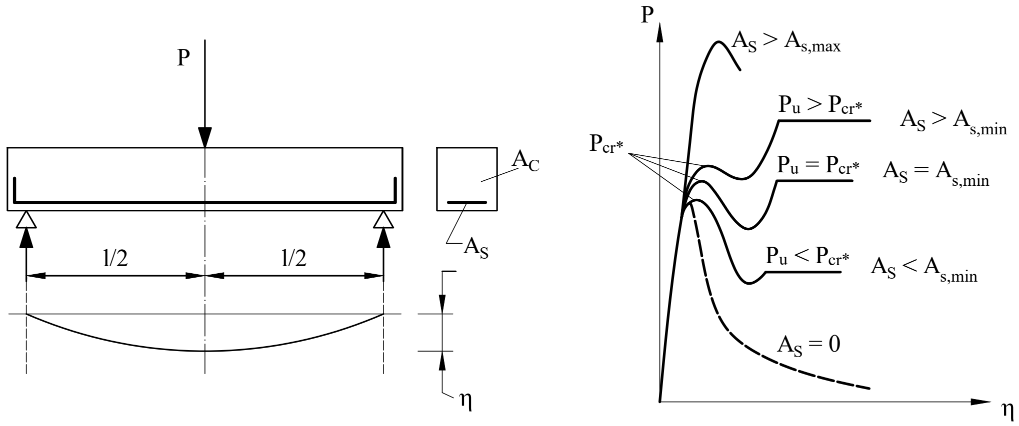

Figure 3.1: Load deflection of beam with different reinforcements

Therefor, the beam reinforcement should be in between the minimum and the maximum:

$$Amin \leq As \leq Amax$$

Which in terms of reinforcement ratio is as follows:

$$\rho, min \leq \rho \leq \rho, max$$

To be $\rho, min \leq \rho \leq \rho, max$ the following inequality should be satisfied:

$$0.11 \leq \xi \leq 0.25$$

where $\xi = y0/d$, which is the coefficient of the neutral axis position, y0 is the distance from the the top fiber to the neutral axis, and d is the distance from the top fiber to the reinforcement, as shown in the figure 3.2.

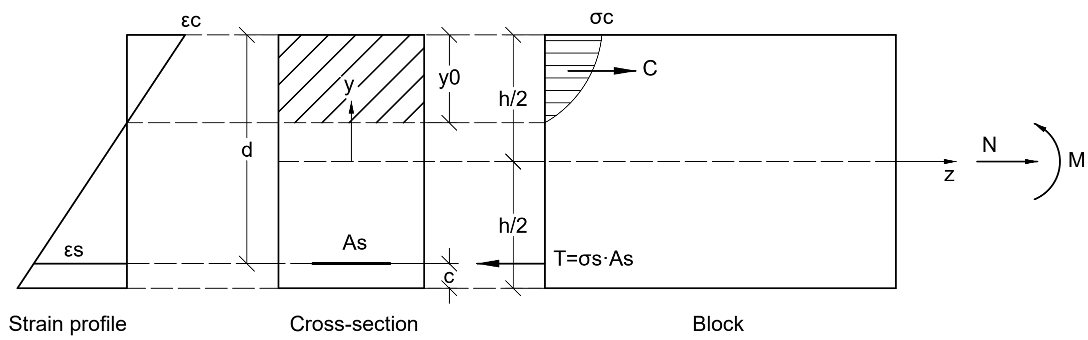

Figure 3.2: Neutral axis position coefficient

Therefor, we can choose to be in the field 3 configuration, shown in the figure 3.3.

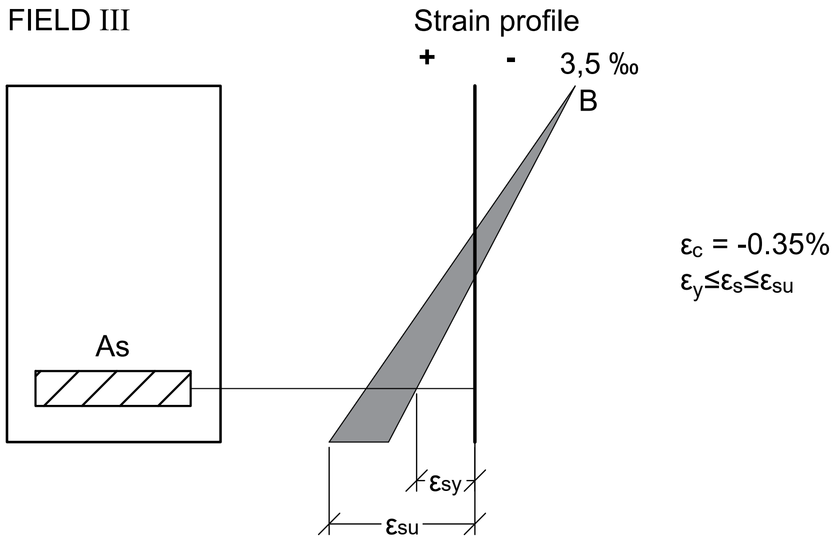

Figure 3.3: Field 3 configuration

If we choose to be in the field 3 we will have the following equations:

$$\omega = 0.81 \cdot \xi$$

$$\mu_{Rd} = 0.81 \cdot \xi \cdot (1 - 0.42 \cdot \xi)$$

In GFRP reinforced concrete we have no ductility since GFRP are not ductile, the reinforcement failure is also brittle, therefor, we do not have limitation of ξ.

3.1 Calculation models for GFRP reinforced concrete beams

A numerical simulation is performed using moment-curvature relationship, using stess-strain laws ($\sigma - \varepsilon$).
The following assumptions are made:

- Pre-peak branch of Sargin parabola is used for concrete.
- There is no tension resistance in concrete.
- $\sigma - \varepsilon$ relationship of GFRP is linear.

From the numerical simulation, given section and materials properties, data reported in the table 3.1, by using the following equation, are calculated ξ, μ_{Rd} and ω, which are respectively the neutral axis position coefficient, the curvature, and the percentage of the reinforcement.

$$\xi = y0/d \tag{3.1}$$

$$\mu_{Rd} = \frac{Mrd}{f_{cm} \cdot b \cdot d^2} \tag{3.2}$$

$$\omega = \frac{Af \cdot f_u}{b \cdot d \cdot f_{cm}} \tag{3.3}$$

Where:

- b = Width of the Beam;
- Af = Area of GFRP bars;
- $y0$ = Distance from the top fiber to the neutral axis;
- d = Distance from the top fiber to the reinforcement;
- f_{cm} = Concrete compressive strength;
- f_u = Ultimate strength of GFRP .

In particular, were calculated the theoretical curvature, the experimental curvature, and these were respectively derived as follows:

$$\mu_{th} = \frac{Mth}{f_{cm} \cdot b \cdot d^2} \tag{3.4}$$

$$\mu_{exp} = \frac{Mexp}{f_{cm} \cdot b \cdot d^2} \tag{3.5}$$

Where the theoretical moment Mth is calculated as:

$$Mth = 0.9 \cdot Af \cdot d \cdot fu \tag{3.6}$$

Which is used to derive the extent till which this equation can be adopted and to **derive the "new" formula**.
Furthermore a curvature were obtained from the moment curvature relationship, reported as $\mu *$.

Calculated values of $\xi, \mu th, \mu exp, \mu *$ and ω are reported in the table 3.2

Article		Specimens	h (m)	b (m)	d (m)	Mu exp (kN . m)	f'c (MPa)	fu (MPa)	Af mm^2
Sehab Mehany et. al.		GI 4#6	0.3	0.2	0.24045	85.61	43	1382	1146
		GI 3#6			0.24045	89.04	43.8	1382	860
		GI 3#5			0.25405	81.36	43.8	1451	596
		GI 2#5			0.25405	67.83	43.8	1451	397
		GII 3#5			0.25405	78.59	43	1245	596
		GII 2#5			0.25405	65.67	43	1245	397
		N GI 3#5			0.25405	81.72	41.3	1451	596
H. Falah Hassan et. al.		B2	0.2	0.15	0.165	23.81	32	1200	308
		B3			0.165	40.36	32	1200	462
Mohamed S. M. & A. Fawzi		B2	0.2	0.15	0.157	27.40	30	407	314
		B5			0.157	35.50	60	407	314
SUNGWOO SHIN et. al.		FB02	0.4	0.3	0.35412	68.94	30	690	253
		FB03			0.35412	111.18	30	690	380
		FB04			0.35412	125.88	30	690	507
		FB06			0.35412	171.54	30	690	760
		FB08			0.35412	222.60	30	690	1013
El-Nemr et. al.	series 1	3 # 13 G1	0.4	0.2	0.3435	80.30	33.5	817	398
		5 # 13 G1			0.3435	129.63	38.95	817	664
		2 # 13 G2			0.3435	80.51	33.5	1639	265
	series 2	3 # 15 G1			0.3425	71.44	38.95	751	530
		4 # 15 G1			0.3425	138.22	38.95	751	707
		2 # 15 G2			0.3425	94.26	29	1362	353
		2 # 15 G3			0.3425	94.84	33.83	1245	353
	series 3	6 # 15 G1			0.32	115.21	33.5	751	1060
		5 # 15 G2			0.32	125.84	29	1362	884
		5 # 15 G3			0.32	112.01	33.8	1245	884
	series 4	2 # 20 G1			0.34	71.90	38.95	728	628
		3 # 20 G1			0.34	139.21	42.1	728	942
		3 # 20 G2			0.34	169.17	48.13	1082	760
		2 # 22 G1			0.339	100.53	38.95	693	942
	series 5	2 # 25 G1			0.3375	160.77	48.13	666	982
		2 # 25 G2			0.3375	173.66	48.13	1132	982
		2 # 25 G3			0.3375	107.93	33.8	906	982
M. Pecce et. al.		F1	0.185	0.5	0.145	57.71	30	600	507
		F			0.145	33.23	30	600	887
A. Ramachandra et. al.		GFRP-S-13	0.2	0.1	0.1605	19.29	40	673	265

h = Overall depth
b = Width
Mu. exp = Experimental Ultimate moment
f'c = Concrete compressive strength
fu = Ultimate strength of GFRP

Table 3.1: Data collected from articles

Article		Specimens	ξ	$\mu*$	ω	μ_{th}	μ_{exp}
Sehab Mehany et. al.		GI 4#6	0.301562	0.175117	0.775451	0.689357	0.172178
		GI 3#6	0.265692	0.158151	0.570965	0.507574	0.175805
		GI 3#5	0.22888	0.13761	0.411099	0.349536	0.143903
		GI 2#5	0.192871	0.116737	0.274066	0.233024	0.119972
		GII 3#5	0.221348	0.133429	0.359338	0.305492	0.141589
		GII 2#5	0.186516	0.11298	0.239559	0.203661	0.118312
		N GI 3#5	0.23259	0.140534	0.435983	0.370694	0.153289
H. Falah Hassan et. al.		B2	0.237102	0.139863	0.466631	0.419831	0.182217
		B3	0.27896	0.163371	0.699946	0.629747	0.308844
Mohamed S. M. & A. Fawzi		B2	0.208206	0.116794	0.085281	0.162883	0.247024
		B5	0.16538	0.064652	0.04264	0.081441	0.160025
SUNGWOO SHIN et. al.		FB02	0.107732	0.061107	0.05493	0.049366	0.061084
		FB03	0.126999	0.073977	0.082396	0.074049	0.098511
		FB04	0.143157	0.084214	0.109861	0.098732	0.111536
		FB06	0.169593	0.100471	0.164791	0.148097	0.151992
		FB08	0.191016	0.113511	0.219721	0.197463	0.197234
El-Nemr et. al.	series 1	3 # 13 G1	0.157878	0.097163	0.14146	0.127222	0.101574
		5 # 13 G1	0.185649	0.115433	0.202878	0.182367	0.141033
		2 # 13 G2	0.152842	0.093257	0.189169	0.170148	0.101839
	series 2	3 # 15 G1	0.168586	0.103842	0.148946	0.134301	0.078182
		4 # 15 G1	0.1894	0.118091	0.198649	0.179068	0.151257
		2 # 15 G2	0.18024	0.11462	0.241793	0.218089	0.138541
		2 # 15 G3	0.162713	0.100438	0.189479	0.170892	0.119488
	series 3	6 # 15 G1	0.224451	0.134634	0.173731	0.334258	0.167921
		5 # 15 G2	0.252642	0.155822	0.363748	0.583558	0.211877
		5 # 15 G3	0.228459	0.138736	0.285302	0.457675	0.161818
	series 4	2 # 20 G1	0.180719	0.112127	0.172938	0.155431	0.079842
		3 # 20 G1	0.207335	0.128622	0.239998	0.215702	0.143017
		3 # 20 G2	0.210114	0.128512	0.311871	0.226209	0.152029
		2 # 22 G1	0.193545	0.120713	0.199796	0.222592	0.112295
	series 5	2 # 25 G1	0.215561	0.131915	0.201561	0.181133	0.146627
		2 # 25 G2	0.236143	0.144352	0.342381	0.307871	0.158381
		2 # 25 G3	0.248534	0.15809	0.390289	0.350873	0.140166
M. Pecce et. al.		F1	0.175869	0.100302	0.140014	0.125803	0.182986
		F	0.217861	0.127379	0.245025	0.220156	0.105369
A. Ramachandra et. al.		GFRP-S-13	0.226519	0.13173	0.278696	0.250455	0.1872

Table 3.2: Calculated variables for numerical simulation

3.1.1 Relationship between ω and ξ for GFRP reinforced beams

From the obtained results by the analyzed beams, the relationship between ω and ξ is derived for the beams reinforced with GFRP.

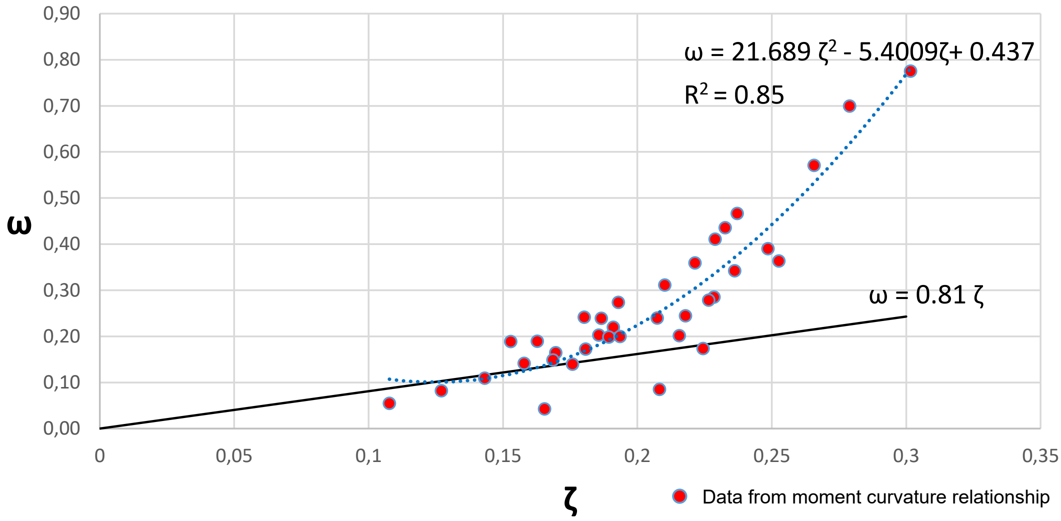

Figure 3.4: Reinforcement percentage - Neutral axis coefficient plot

In fact, ω and ξ values are plotted in the figure 3.4, the plot shows, the relationship $\omega = 0.81 \cdot \xi$ is valid for the following ξ values:

$$0.12 \leq \xi \leq 0.17$$

For ξ values greater than 0,17 the following relation is valid, derived from an interpolation of the data.

$$\omega = 21.689 \cdot \xi^2 - 5.4009 \cdot \xi + 0.437 \tag{3.7}$$

3.1.2 Relationship between μ_{Rd} and ξ for GFRP reinforced beams

The $\mu - \xi$ relationship is completely different from the relationship we have for steel reinforced concrete, which is the following:

$$\mu_{Rd} = 0.81 \cdot \xi(1 + 0.42 \cdot \xi)$$

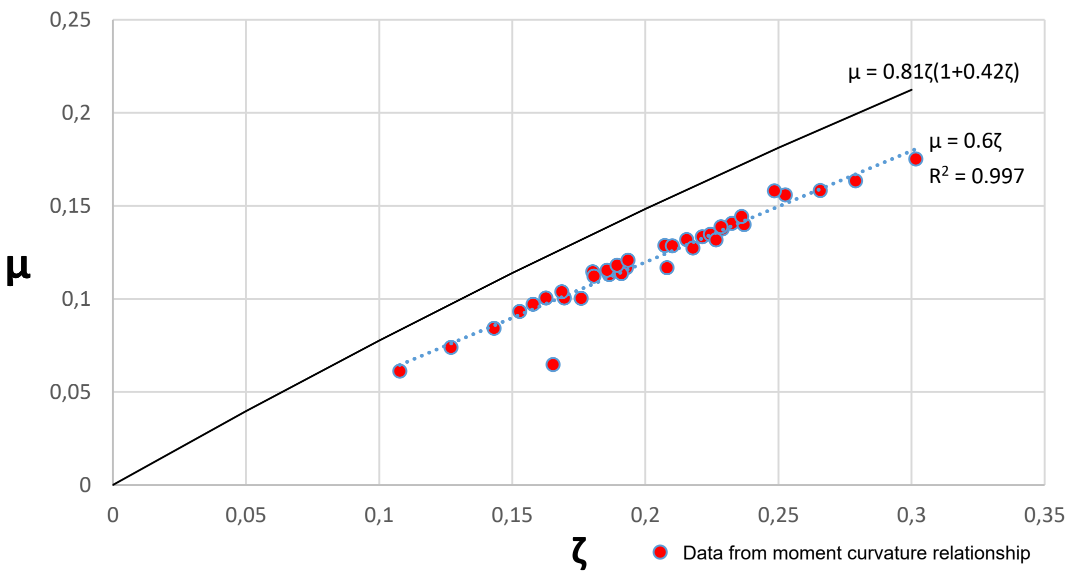

Figure 3.5: Curvature (μ) - Neutral axis coefficient (ξ) plot

For the analyzed beams the curvature against neutral axis coefficient values are plotted in the figure 3.5.

The new relationship found is almost linear as it can be seen by the figure 3.5, for any value of ξ, which is the following:

$$\mu_{Rd} = 0.6 \cdot \xi \tag{3.8}$$

This relation proves us that for the given ξ value, μ_{Rd} value is lower in the GFRP reinforced concrete beams, with respect to the steel reinforced beams.

3.1.3 Resisting moment formulation for GFRP reinforced beams

Furthermore, from the equation 3.8 by using the equation 3.2 we have the following relationship:

$$\frac{Mth}{f_{cm} \cdot b \cdot d^2} = 0.6 \, \frac{y0}{d}$$

Therefor, we retrieve the following relationship:

$$M_{Rd} = 0.6 \cdot b \cdot d \cdot y0 \cdot fcm \tag{3.9}$$

By introducing the following simplification: $C = fcm \cdot y0 \cdot b$, therefor, having the configuration shown in the figure 3.6.

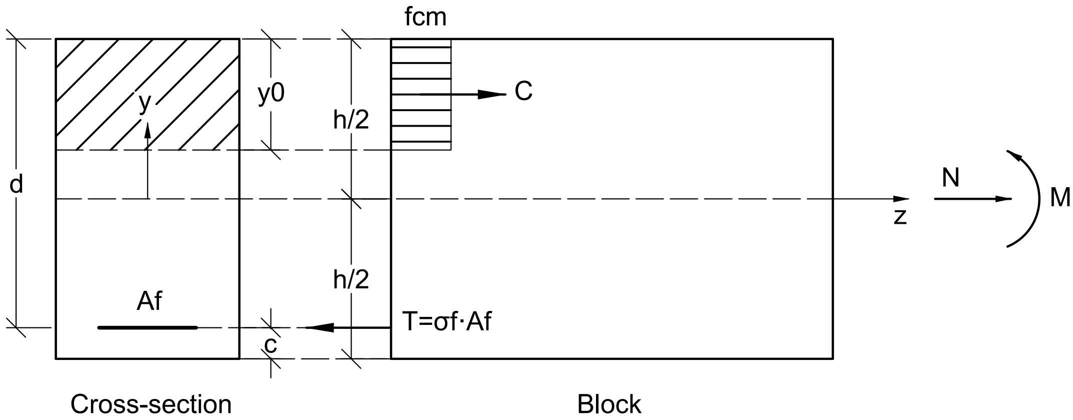

Figure 3.6: Simplified configuration

Therefor, for equilibrium we will have $C == T$, where $T = \sigma_f \cdot A_f$ for GFRP reinforced beams.

Finally we have:

$$M_{Rd} = 0.6 \cdot d \cdot \sigma_f \cdot A_f \tag{3.10}$$

σ_f is lower or equal to f_u.

As a result, for the same reinforcement, the resisting moment of concrete beams reinforced with GFRP is less than that of steel reinforced beams.

3.1.4 Relationship between μ_{Rd} and ω

Integrating the equation 3.7 and the equation 3.8 as follows:

$$\begin{cases} \omega = 21.7 \cdot \xi^2 - 5.4 \cdot \xi + 0.44 \\ \mu_{Rd} = 0.6 \cdot \xi \end{cases}$$

Which is equal to:

$$\begin{cases} \xi = \mu_{Rd}/0.6 \\ \omega = 21.7/0.6^2 \cdot \mu_{Rd}^2 - 5{,}4/0{,}6 \cdot \mu_{Rd} + 0{,}44 \end{cases}$$

Therefor, we have:

$$\mu_{Rd}^2 \cdot a + \mu_{Rd} \cdot b + c = 0$$

$a = 21.7/0.6^2 = 60.3$

$b = -9$

$c = 0.44 - \omega$

$$\mu_{Rd} = \frac{-b \pm \sqrt{b^2 - 4ac}}{2 \cdot a}$$

$b^2 - 4ac \geq 0$

$81 - 4 \cdot 60.3(0.44 - \omega) \geq 0$

Therefor, $\omega \geq 0.11$

Finally we can state that if $\omega \geq 0{,}11$ we have the following equation:

$$\mu_{Rd} = \frac{-9 \pm \sqrt{241.2 \cdot \omega - 25.1}}{120.6}$$

This equation gives us two solutions, the greater one should be considered, therefor, we have the following relation:

$$\mu_{Rd} = \frac{-9 + \sqrt{241.2\omega - 25.1}}{120.6} \tag{3.11}$$

Therefor, based on values obtained from moment-curvature relationship, we have this new relationship, which can be seen in the figure 3.7.

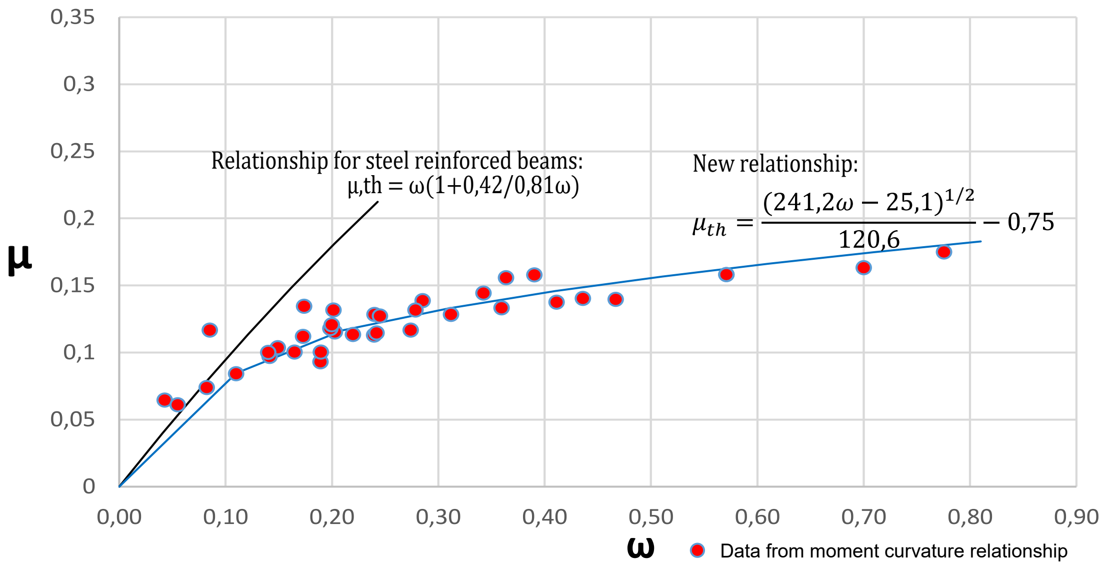

Figure 3.7: $\mu - \omega$ relationship for GFRP

Chapter 4

The comparison between the computation model and the experimental results

The models found are compared with the experimental values retrieved in the literature for the validation.

For instance, hereafter, μ and ω relationship obtained with moment-curvature relationship is compared with the experimental μ and ω values, shown in the figure 4.1.
μ_{Rd} should have σ, cd rather than fcm, indeed:

$$\mu_{Rd} = \frac{M_{Rd}}{b \cdot d^2 \cdot \sigma cd} \tag{4.1}$$

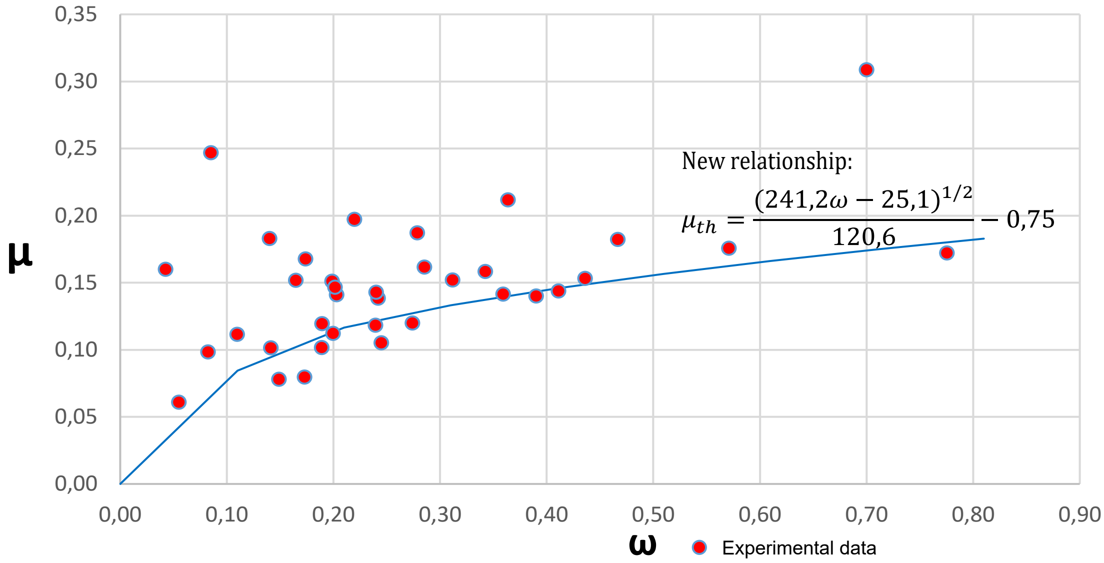

Figure 4.1: $\mu - \omega$ comparison with experimental data

$$\sigma cd = \frac{0.85 \cdot fck}{1.5} \tag{4.2}$$

$fck = fcm - 8;$

Therefor, a coefficient α is calculated as $fcm/\sigma cd$ to be multiplied by μ to correct the μ values.

$$\alpha = \frac{fcm}{\sigma cd} = \frac{fcm \cdot 1.5}{0.85 \cdot (fcm - 8)} \tag{4.3}$$

For $fck = 25$ we find α to be 3.33.

For $fck = 50$ we find α equal to 2.17, hereafter α is considered to be equal to 2. The comparison is shown in the figure 4.2

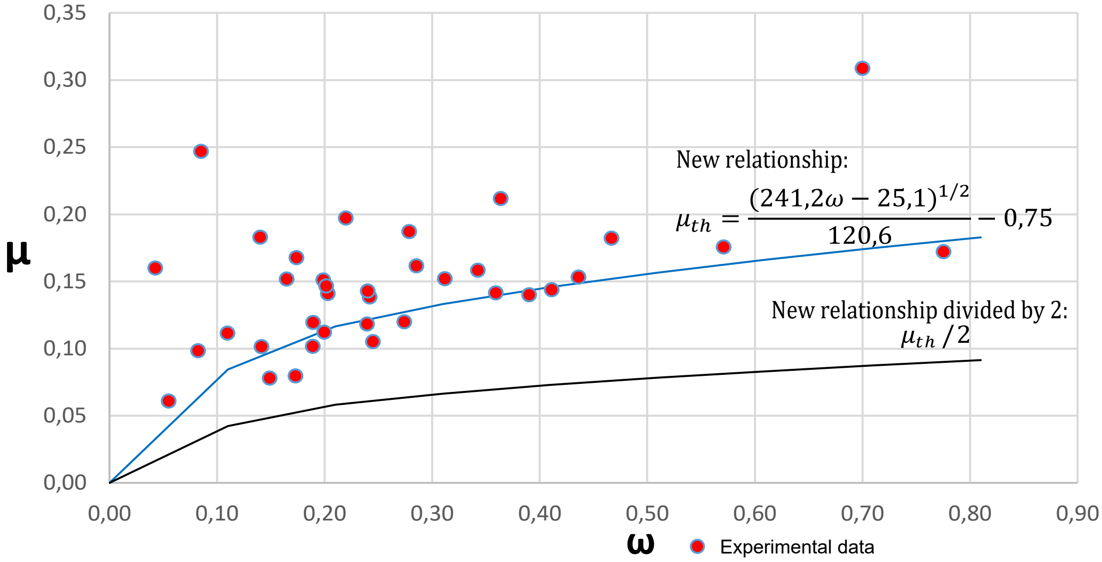

Figure 4.2: $\mu_{Rd} - \omega$ comparison with experimental data

The formulation within the safety format of the model code and Euro Code 2 (limit states) is in favor of safety, always providing a maximum moment lower than the experimental moment.

Hereafter a comparison is provided between the experimental moment and the theoretical moment calculated as:

$$M_{R,th} = 0.6 \cdot Af \cdot fud \cdot d$$

The comparison is shown in the figure 4.3.

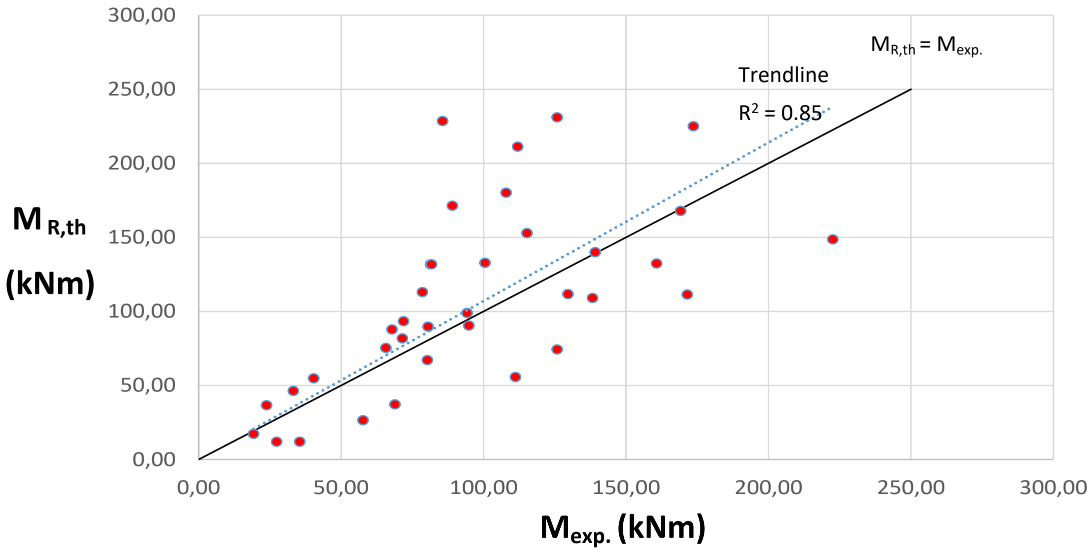

Figure 4.3: $M_{R,th} - M_{exp.}$ plot

We can observe that despite the dispersion of the points, the trend line is close to the line $M_{exp.} = M_{R,th.}$.
Lastly, a plot of M_R obtained from moment curvature relationship against $M_{exp.}$ is shown in the figure 4.4.
Finally we can state that analysis done with moment curvature relationship is very reliable since the data is close to the line $M_R - M_{exp.}$

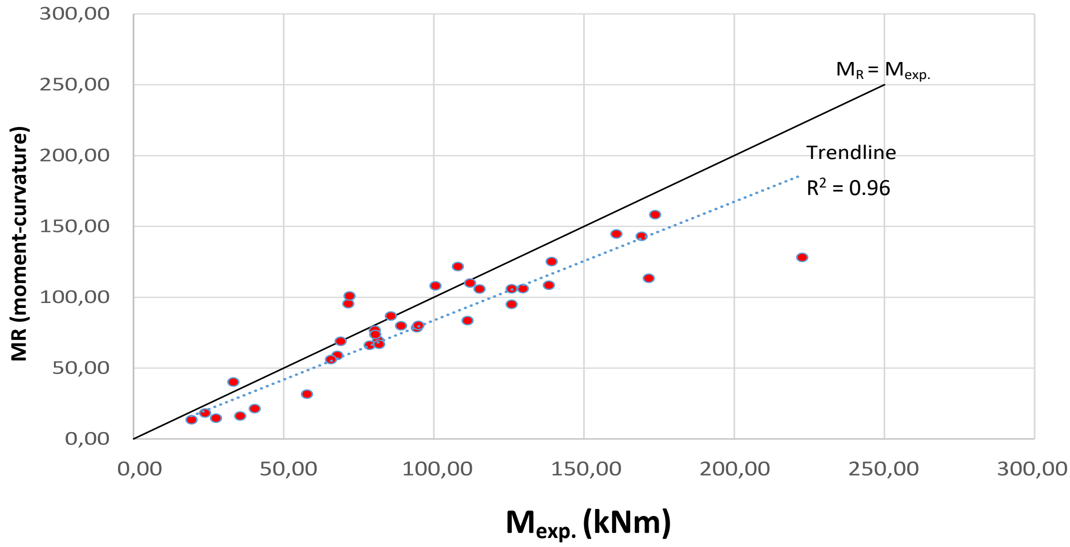

Figure 4.4: $M_{R,moment-curvature} - M_{exp.}$ plot

Chapter 5

Conclusions

The primary purpose of this research is to provide some formulas for calculating the main variables we have when design by flexure.
The following conclusive statements can be made:

- For the beams reinforced with GFRP, the ω-ξ relationship is different from the steel reinforced beams, it is not linear anymore, it has a parabolic relationship, as follows:

$$\omega = 21.689 \cdot \xi^2 - 5.4009 \cdot \xi + 0.437$$

- The μ_{Rd} and ξ relationship is again different for GFRP reinforced beams from the classical steel reinforced beam. μ_{Rd} is lower for GFRP reinforced beams. We have the following relationship:

$$\mu_{Rd} = 0.6 \cdot \xi$$

- The μ_{Rd} and ω relation is different as well, which is the following:

$$\mu_{Rd} = \frac{-9 + \sqrt{241.2\omega - 25.1}}{120.6}$$

Therefor, to have the same μ_{Rd} we need higher reinforcement percentage.

- The formula retrieved for GFRP reinforced beam is the following:

$$M_{Rd} = 0.6 \cdot fud \cdot A_f \cdot d$$

Therefor, the coefficient is no longer 0.9 as for steel reinforced concrete, it is 0.6. This doesn't necessary means that more reinforcement is needed to reach the same resistance since it depends also on the fud which can be much more greater than the steel. Rather than fyd we have fud.

Bibliography

[1] MEPS INTERNATIONAL. *How did prices reach record highs during a pandemic?* URL: https://mepsinternational.com/gb/en/news/how-did-steel-prices-reach-record-highs-during-a-global-pandemic (cit. on pp. 4, 6, 7).

[2] LAVORI PUBBLICI. *Acciaio: Prezzi in aumento dopo lo shock della guerra.* Mar. 2022. URL: https://www.lavoripubblici.it/flash-news/2022/03/Acciaio-prezzi-in-aumento-dopo-lo-shock-della-guerra-1797.html (cit. on p. 8).

[3] RICCARDO SAPORITI. *Quanto dipendiamo da gas E petrolio dalla russia?* Mar. 2022. URL: https://www.wired.it/article/gas-petrolio-russia-dipendenza-europa/ (cit. on p. 8).

[4] MARGHERITA COLDANI. *Assolombarda - Conflitto Russia-Ucraina, Spada: "Cresce Il Costo dell'energia".* Mar. 2022. URL: https://www.assolombarda.it/media/comunicati-stampa/conflitto-russia-ucraina-spada-201ccresce-il-costo-dell2019energia-per-le-industrie-manifatturiere-della-lombardia-passando-da-8-3-miliardi-di-euro-a-11-5-nel-2022-in-due-settimane-ora-la-priorita-e-garantire-la-continuita-operativa-delle-imprese201d (cit. on p. 8).

[5] TRADING ECONOMICS. *European Union imports of iron and steel from RUSSIA2022 DATA 2023 Forecast 2000-2021 historical.* URL: https://tradingeconomics.com/european-union/imports/russia/iron-steel (cit. on p. 8).

[6] IMAD ABBOOD et. al. «Properties evaluation of fiber reinforced polymers and their constituent materials used in structures – A review». In: *Materials Today: Proceedings* 43 (Apr. 2021), pp. 1003–1008. DOI: 10.1016/j.matpr.2020.07.636 (cit. on pp. 9, 10).

[7] CNR. *Guide for the Design and Construction of Externally Bonded FRP Systems for Strengthening Existing Structures.* Tech. rep. CNR - Advisory Committee on Technical Recommendations for Construction, 2004 (cit. on p. 10).

[8] B. BENMOKRANE et. al. «Reinforcement of concrete using fibre-reinforced polymer composites». In: *Durability of Composites for Civil Structural Applications.* Ed. by Vistasp M. Karbhari. Woodhead Publishing Series in Civil and Structural Engineering. Woodhead Publishing, 2007, pp. 225–246. ISBN: 978-1-84569-035-9. DOI: https://doi.org/10.1533/9781845693565.2.225. URL: https://www.sciencedirect.com/science/article/pii/B9781845690359500116 (cit. on p. 12).

[9] HAITHAM A. IBRAHIM. «3d fe analysis for the seismic behavior of hybrid steel-frp reinforced concrete beam-column joints». PhD thesis. June 2017. DOI: 10.13140/RG.2.2.16339.84002 (cit. on p. 13).

[10] TUF TUF-BAR. *GFRP vs Black Steel: Fiberglass rebar: TUF-bar.* Feb. 2022. URL: https://www.tuf-bar.com/application/gfrp-vs-steel/gfrp-vs-black-steel/#:~:text=The%20black%20steel%20reinforced%20pad,to%20fatigue%20cracking%20over%20time. (cit. on p. 14).

[11] LE SCIENZE. *Ferro e acciaio, UN Primato da Impatto Ambientale.* URL: https://www.lescienze.it/news/2014/07/16/news/impatto_ambientale_metalli-2215818/#:~:text=La%20produzione%20di%20ferro%20e,serra%20responsabile%20dal%20cambiamento%20climatico (cit. on p. 14).

[12] WORLDSTEEL.org. *Sustainability Indicators 2021 and our sustainability journey.* Tech. rep. World Steel Association, 2021 (cit. on p. 14).

[13] CORDIS. *Major step towards producing carbon-neutral steel with green hydrogen ...* URL: https://cordis.europa.eu/article/id/411733-major-step-towards-producing-carbon-neutral-steel-with-green-hydrogen (cit. on p. 15).

[14] THE WORLD COUNTS. URL: https://www.theworldcounts.com/challenges/planet-earth/mining/environmental-impact-of-steel-production/story (cit. on p. 15).

[15] KRAFTON GFRP. *Krafton® glass fibre-reinforced plastic (GRP) has a low environmental impact*. Sept. 2019. URL: https://www.krafton.uk/grp-profiles/environment/ (cit. on pp. 15, 16).

[16] COMPOSITES UK. *End of life options*. June 2022. URL: https://compositesuk.co.uk/composite-materials/properties/end-life-options (cit. on p. 17).

[17] EL-NEMR AMR et. al. «Evaluation of the flexural strength and serviceability of concrete beams reinforced with different types of GFRP Bars». In: *Engineering Structures* 173 (2018), pp. 606–619. DOI: 10.1016/j.engstruct.2018.06.089 (cit. on pp. 20–27).

[18] M. PECCE et. al. «Experimental response and code MODELSOF GFRP RC beams in bending». In: *Journal of Composites for Construction* 4.4 (2000), pp. 182–190. DOI: 10.1061/(asce)1090-0268(2000)4:4(182) (cit. on pp. 20, 28, 29, 46, 47).

[19] A. RAMACHANDRA MURTHY et. al. «Performance of concrete beams reinforced with GFRP bars under monotonic loading». In: *Structures* 27 (2020), pp. 1274–1288. DOI: 10.1016/j.istruc.2020.07.020 (cit. on pp. 20, 29–32).

[20] SHEHAB MEHANY et. al. «Flexural Strength and Serviceability of GFRP-Reinforced Lightweight Self-Consolidating Concrete Beams». In: *Journal of Composites for Construction* 26.3 (2022), p. 04022020. DOI: 10.1061/(ASCE)CC.1943-5614.0001208 (cit. on pp. 20, 33–36, 47).

[21] H. FALAH HASSAN et. al. «Flexural performance of concrete beams reinforced by GFRP bars and strengthened by CFRP Sheets». In: *Case Studies in Construction Materials* 13 (2020). DOI: `10.1016/j.cscm.2020.e00417` (cit. on pp. 21, 37–39).

[22] MOHAMED S. MOAWAD. «Performance of concrete beams partially/fully reinforced with glass fiber polymer bars». In: *Journal of Engineering and Applied Science* 68.1 (2021). DOI: `10.1186/s44147-021-00028-6` (cit. on pp. 21, 39–42).

[23] SUNGWOO SHIN et. al. «Performance of concrete beams reinforced with GFRP bars». In: *Journal of Asian Architecture and Building Engineering* 8.1 (2009), pp. 197–204. DOI: `10.3130/jaabe.8.197` (cit. on pp. 21, 43–46).